Compositions of Unzoned and Zoned Metal in the CB_b Chondrites Hammadah al Hamra 237 and Queen Alexandra Range 94627

ANDREW J. CAMPBELL[1,*], MUNIR HUMAYUN[2], AND MICHAEL K. WEISBERG[3]

[1]Department of the Geophysical Sciences, University of Chicago, Chicago, IL 60637

[2]National High Magnetic Field Laboratory and Department of Geological Sciences, Florida State University, Tallahassee, FL 32310

[3]Department of Physical Sciences, Kingsborough College of the City University of New York, Brooklyn, NY 11235, and Department of Earth and Planetary Sciences, American Museum of Natural History, New York, NY 10024

*email: a-campbell@uchicago.edu

ph: (773) 834-1523, fax: (773) 702-9505

Submitted to *Meteoritics & Planetary Science* October 5, 2004

Accepted June 1, 2005

Abstract–The CB_b chondrites are rare, primitive, metal-rich meteorites that contain several features, including zoned metal, that has previously been interpreted as evidence for origins in the solar nebula. We have measured concentrations of Ni, Cu, Ga, Ru, Pd, Ir, and Au within both zoned and unzoned metal grains in the CB_b chondrites QUE 94627 and HH 237, using laser ablation inductively coupled plasma mass spectrometry. Refractory elements Ni, Ru, and Ir are enriched in the grain cores, relative to the rims, in the zoned metal. All refractory elements are uniform across the unzoned metal grains, at concentrations that are highly variable between grains. Volatile elements Cu, Ga, and Au are usually depleted relative to chondritic abundances, and are most often uniform within the grains, but sometimes are slightly elevated at the outermost rim. The Pd abundances are nearly uniform, at close to chondritic abundances, in all of the metal grains. A condensation origin is inferred for both types of metal. The data support a model in which the zoned metal formed at high temperatures, in a relatively rapidly cooling nebular gas, and the unzoned metal formed at lower temperatures, and at a lower cooling rate. The CB_b metal appears to have formed by a process very similar to that of the CH chondrites, but the CB_b meteorite components experienced even less thermal alteration following their formation, and are among the most primitive materials known to have formed in the solar nebula.

INTRODUCTION

The study of primitive meteorite components, that have experienced little or no metamorphism after accretion onto their parent bodies, is a principal source of information on the conditions of the solar nebula and processes that occurred therein. Much has been learned about the temperatures and timescales on which matter was processed in the early solar system through the study of, for example, Ca,Al-rich inclusions (CAIs) and chondrules that are found in primitive chondrites. However, chondrules and many CAIs are igneous objects, and their melting and recrystallization have significantly obscured the record of the condensation of these objects, or of their precursors, from the nebular gas. It has recently been recognized (Meibom et al., 1999; 2001; Weisberg et al., 1999; 2001; Campbell et al., 2001; Petaev et al., 2001; 2003; Campbell and Humayun, 2004) that a class of metal grains in some CR-clan primitive meteorites (Weisberg et al., 1995) preserve evidence of gas-solid processes that remain largely undisturbed by subsequent melting or thermal metamorphism. The silicate components in these meteorites also bear evidence of high-temperature condensation processes (Krot et al., 2001; 2002; Hezel et al., 2003). In this study we present new data on zoned and unzoned metal from two meteorites in the CB_b group, Hammadah al Hamra (HH) 237 and Queen Alexandra Range (QUE) 94627 (paired with QUE 94411), that permits an improved understanding of the history of metal condensates.

The CB chondrite group (Weisberg et al., 2001) is characterized by high metal contents and large low-FeO chondrules that usually have cryptocrystalline or barred olivine textures and are rarely porphyritic. The metal exhibits little to no kamacite/plessite decomposition, and some metal contains numerous small sulfide inclusions. The metal and silicate grains are held together by a small proportion of shock-produced melt. The CB group is associated with other CR-clan chondrite classes, including the CH group, on the basis of their similar oxygen and nitrogen isotopic compositions, volatile depletions, and

low degrees of alteration (Weisberg et al., 1995; 2001). Further classification into the CB_a and CB_b subgroups was advocated by Weisberg et al. (2001) on the basis of important textural/compositional differences, including the presence of zoned metal grains in the CB_b members (HH 237 and QUE 94411, paired with QUE 94627) that are missing from the CB_a members (Bencubbin, Gujba, and Weatherford), and which may reflect important genetic differences (Campbell et al., 2002).

Weisberg et al. (1999) noted that chondritic Ni/Co ratios in QUE 94411 are suggestive of nebular processing of the metal, probably a volatility-controlled process such as condensation or evaporation. Meibom et al. (1999) highlighted the fact that a set of zoned metal grains in the CH chondrites Pecora Escarpment (PCA) 91467 and Patuxent Range (PAT) 91546 contains rim-to-core compositional sequences of P, Cr, Co, and Ni that parallel that which is expected from equilibrium calculations of metallic alloy condensation in the solar nebula (Grossman and Olsen, 1974; Grossman et al., 1979; Kelly and Larimer, 1977). Campbell et al. (2001) measured trace siderophile element distributions within similarly zoned metal in QUE 94411 and confirmed that the elemental fractionations within those grains were volatility-controlled, and not the product of redox processing, which could not be strictly excluded on the basis of the Meibom et al. (1999) results alone. Campbell et al. (2002) investigated trace siderophile element distributions in the CB_a chondrites Bencubbin, Gujba, and Weatherford, and demonstrated that intergrain variations of trace element abundances in the metal in these meteorites suggested an origin by volatilization/condensation, but is different from the trends observed in zoned metal in QUE 94411. A non-nebular origin of this metal, consistent with that proposed by Kallemeyn et al. (2001), was suggested. Campbell and Humayun (2004) extended these measurements to zoned metal in CH chondrites, demonstrating that those grains formed by a process indistinguishable from that of the zoned metal in QUE 94411, apart from the mean grain size being significantly smaller in the CH metal. Campbell and Humayun (2004) further elucidated the relationship between the zoned and unzoned metal in the CH chondrites,

demonstrating that there is a complementary relationship in their trace element abundances, and that the unzoned metal is not simply a homogenized form of the zoned metal.

Theoretical models of the formation of the zoned metal in CB and CH chondrites have progressed along with the increasingly detailed analytical work, and new experimental work should further improve these models. Meibom et al. (1999) originally interpreted the zoning as a sequence of compositions following an equilibrium condensation trajectory. The cooling rate of the condensing gas was then calculated by correlating the change in composition, hence temperature, with the rate of grain growth as calculated using kinetic theory of gases. Petaev et al. (2001) expanded upon this model, incorporating the roles of variable oxygen fugacity, rates of sequestration of the metal from the gas, and depletion of Cr. The presence of substantial refractory PGE contents throughout the grains, even outside their innermost cores, led Campbell et al. (2001) to remark on the apparent absence of reservoir effects associated with fractional condensation, that would have been expected from the scenario proposed by Meibom et al. (1999). Campbell et al. (2001) proposed two models, that are not exclusive of one another, that satisfy the observed compositional zoning: (1) condensation from a supersaturated gas, such that most of the refractory siderophile budget remained in the gas and was therefore available for later condensation into subsequent shells of the growing grains, and (2) condensation of Fe-Ni metal onto a refractory-enriched core, followed by diffusion of refractory siderophiles outward from the core into the later-deposited metal. Petaev et al. (2003) developed a grain growth model that incorporates both of these processes, and concluded that both diffusion and the change in alloy composition with condensation temperature (T_c) are important factors in the establishment of the zoned profiles. Righter et al. (2005) have experimentally determined diffusion rates of several siderophile elements in metal, using natural abundance levels to improve accuracy and also to facilitate interelement comparisons for application to the zoned metal in CB_b and CH chondrites. Campbell and Humayun (2004) discussed the nature of multiple, transient heating/cooling events in the solar nebula, with variable timescales, peak

temperatures, and metal sequestration temperatures, that could have produced both the zoned and unzoned metal found in CH chondrites. Campbell and Humayun (2004) also noted that, in addition to plessitic decomposition in some of the Fe-Ni grains, details of the Cu distribution in both zoned and unzoned metal provide evidence for parent body metamorphism in the CH chondrites.

In this contribution, we present profiles of Ni, Cu, Ga, Ru, Pd, Ir and Au concentrations for both zoned and unzoned metal grains in HH 237 and QUE 94627. The inclusion of Cu, Ga, and Au significantly expands the list of volatile siderophile elements for which zoned CB_b metal has been analyzed. In addition, an emphasis in the present work on unzoned metal in the CB_b chondrites permits the relationship between zoned and unzoned metal to be examined in a way similar to that in which Campbell and Humayun (2004) studied metal in CH chondrites, and facilitates a comparison between the history of CB_b and CH metal.

EXPERIMENTAL

A section of HH 237 (AMNH 4956) was obtained from the American Museum of Natural History, and section QUE 94627,4 was obtained from the United States Antarctic Meteorite Collection. We examined the specimens optically, and studied them using a JEOL 5800LV scanning electron microscope (SEM) with an Oxford Link/ISIS EDX system. Elemental (Kα) X-ray maps were collected using the Cameca SX100 electron microprobe at the American Museum of Natural Histoy. The metal grain sizes in CB_b chondrites are relatively large, and range up to ~700 μm in the sections studied. Compositional profiles across many of the largest (≥150 μm) metal grains in the sections were determined by EDX; these revealed whether or not a particular grain was of the zoned or unzoned variety, and its Ni content. On the basis of this information, we selected individual metal grains for siderophile element analysis by LA-ICP-MS.

The laser ablation system at the University of Chicago utilized a CETAC LSX-200 laser ablation peripheral with a ThermoFinnigan Element ICP mass spectrometer (Campbell and Humayun, 1999; Campbell et al., 2001; 2003). The standard 5× objective lens in the LSX-200 has been changed to a 10× lens, providing greater power density and sensitivity (Campbell et al., 2003). Argon gas is used to carry the ablated material through tygon tubing from the sample chamber of the LSX-200, to a 50 ml Savillex spray chamber, and then to the ICP. The purpose of the spray chamber is to extend the duration over which the laser-ablated material is measured by the ICP-MS. With no spray chamber a transient signal from the LSX-200 passes through the ICP-MS in ~10 s (Campbell and Humayun, 1999), but the 50 ml spray chamber spreads the signal over ~20 s, which we have found to be a satisfactory compromise between signal longevity and minimization of accumulated background.

We optimized the analyses for spatial resolution and sensitivity by reducing the laser spot size to either 25 μm diameter, ~15 μm depth or 13 μm diameter, ~10 μm depth,

and restricting the number of isotopes that were analyzed. Each grain was analyzed at a series of points, located sequentially across the width of the grain in 15 to 30 μm steps. Most of the LA-ICP-MS analyses measured ^{57}Fe, ^{60}Ni, ^{63}Cu, ^{69}Ga, ^{101}Ru, ^{105}Pd, ^{193}Ir, and ^{197}Au; these elements were selected to represent a range of volatilities (volatile – Cu, Ga, Au; refractory – Ru, Ir) and chemical affinities (moderately siderophile – Fe, Ga; chalcophile – Cu). Each analyzed point was ablated by 20 to 30 laser pulses at 10 Hz. The mass spectrometer was swept repeatedly over the intended mass range while the ablated material was carried by Ar gas from the sample chamber to the mass spectrometer. The signal from the transient laser ablation pulse was integrated over a period of ~20 s; this was sufficient time for the pulse to reach a peak intensity and then decay almost to background levels.

Blank subtractions (average of 3 measurements with the laser off) were made, and interference corrections for ^{40}Ar^{61}Ni on ^{101}Ru and ^{40}Ar^{65}Cu on ^{105}Pd were also done, although these were found to be negligible (e.g., Righter et al., 2004). Instrumental sensitivity factors for each isotope were determined by measuring signal intensity from the group IIA iron meteorite Filomena, which has known concentrations of the elements of interest (Wasson et al., 1989; Campbell et al., 2002). The intensity data for each analysis were blank-subtracted and then corrected for the instrumental sensitivity factors. Laser ablation ICP-MS requires an internal calibrant. In the present case, because it is known that the target is a ferrous alloy, the internal calibrant was the sum of major elements Fe and Ni; in other words, we normalized the corrected intensity data to [Fe]+[Ni]=100%. Previous comparison between several standards (Campbell et al., 2002) has shown the reliability of this method. Detection limits for each analysis were based on the 3σ standard deviation of the three blank measurements.

Reported concentration data for unzoned grains are means and standard errors of *n* measurements made across the diameter of each grain. The number of points *n* ranged from 6 to 32, and was dependent upon the grain diameter and the spot size used (25 μm or 13 μm). Analytical uncertainties on the unzoned grains were mostly 2% to 8%, but at low

concentrations the precisions were poorer. Detection limits of the unzoned grain averages were reduced by $\sqrt{n}$ from the detection limits of individual analyses. Uncertainties of individual LA-ICP-MS analyses in profiles of zoned grains reflect contributions from counting statistics as well as an instrumental error that is largely due to the transience of the signal. The counting errors incorporate both the measured counts and the counts in the blank measurement. The instrumental error was calculated from repeat measurements of the standards, by stripping away the counting errors from the variance of the standard analyses. This is a conservative estimate of the instrumental error because it assumes homogeneity in the standards, which are known to have fine scale heterogeneities. Instrumental errors (1σ) were assigned as 9.2%; this is the average value from several different calibrations.

RESULTS

Metal in HH 237 and QUE 94627 occurs as three major textural types: (1) large millimeter-size aggregates, (2) small (up to ~300 mm) homogeneous (unzoned), irregular-shaped metal and (3) small compositionally zoned metal (Weisberg et al., 2001). The latter two types are shown in Figure 1. Electron microscope examination of the sections revealed that sulfide inclusions occur in the large metal aggregates and in some of the unzoned metal (Fig. 1). Silicate inclusions also occur in some metal grains, but no dissolved silicon was detected in the metal. Sulfide inclusions were not found in any of the zoned metal studied. An accurate measure of the sulfur content of the unzoned grains is difficult because of the heterogeneous distribution of their sulfides (Figure 1), so in this work we have settled for a coarse categorization of the sulfur contents. In Table 1, each unzoned metal grain has been identified as either "S-rich," indicating the presence of sulfide inclusions, or "S-poor," indicating that one or no sulfide inclusions were observed in the grain. None of the grains analyzed in this study are the large metal aggregates, commonly 1-5 mm in size, that were described by Weisberg et al. (2001). However, it is not known whether some of the S-rich metal grains are fragments from large metal aggregates.

The metal grains that are unzoned in Ni were mostly found to be unzoned in the analyzed trace elements too; an example is shown in Fig. 2a, where it is seen that Cu, Ga, Ru, Pd, Ir, and Au concentrations across grain #hh35c in HH 237 are uniform to within analytical precision. There were several exceptions of the sort represented by grain #que57b in Fig. 2b, in which minor enrichments in Cu and/or Ga were detected at the outer rim of otherwise homogeneous grains. Average compositions for 30 unzoned grains, 25 in HH 237 and 5 in QUE 94627, are given in Table 1, and their trace element abundances are plotted against Ni in Fig. 3. The three volatile elements Cu, Ga, and Au all show similar trends of decreasing abundances with increasing Ni. There is a positive correlation among these elements in the unzoned metal (Fig. 4). The Cu/Au ratio is subchondritic in volatile-

depleted metal but converges toward the chondritic ratio with increasing Au. The Ga/Au ratio is subchondritic in all metal analyzed. Palladium varies only a small amount between grains and is correlated with Ni (Fig. 3). The refractory elements Ru and Ir behave in similar ways but do not correlate strongly with Ni (Fig. 3). The Ru/Ir ratios are uniformly close to the chondritic value, as indicated in Fig. 5a. The refractory elements and the volatile elements show only a weakly negative correlation, as shown in the representative case of Au vs. Ir in Fig. 5b.

Those metal grains that are zoned in Ni are likewise zoned in the other refractory siderophile elements. Trace element profiles from a representative zoned metal grain are shown in Fig. 2c, and data for 7 zoned grains in HH 237 and 2 in QUE 94627 are compiled in the Appendix. As shown in Fig. 2c, these zoned metal grains are convexly zoned (enriched at the core) in Ru and Ir, but the Pd concentrations are nearly uniform. Volatile element (Cu, Ga, Au) abundances are commonly uniform and low, sometimes even below detection limits, and sometimes show higher concentrations toward the rims, as in the example of Fig. 2c. The trace element analyses from all 9 zoned metal grains in this study are plotted against Ni in Fig. 6. The refractory siderophiles Ru and Ir show positive correlations with Ni in these grains. There is less variation in the Pd abundances, but enough to detect a slight positive trend with Ni here too (Fig. 6). The Cu/Ni, Ga/Ni, and Au/Ni ratios are all well below chondritic, and correlations between these volatile elements and Ni are less well defined (Fig. 6).

DISCUSSION

Zoned Metal Grains

The zoning of refractory siderophile elements in HH 237 and QUE 94627 (e.g., Fig. 2) is indistinguishable from that reported for the related meteorite QUE 94411 (Campbell et al., 2001); the same observation for zoned metal in HH 237 had been noted earlier by Campbell et al. (2000). As discussed by Campbell et al. (2001) and Campbell and Humayun (2004), there are two mechanisms that could produce the zoning observed in these refractory siderophiles: (1) condensation from a supersaturated gas, such that most of the refractory siderophile budget remained in the gas while cooling and was therefore available for later condensation into subsequent shells of the growing grains, and (2) condensation of Fe-Ni metal onto a refractory-enriched core, followed by diffusion of refractory siderophiles outward from the core into the later-deposited metal. It is possible, perhaps likely, that the grains formed by some superposition of these two mechanisms, in which diffusion redistributed the siderophiles internal to the grain while it was growing by condensation in a supersaturated gas (Campbell et al., 2001; Petaev et al., 2003).

In Fig. 6 the data from the zoned metal grains are compared to an equilibrium condensation calculation for a metal alloy condensing in a solar gas at 10 Pa total pressure. This calculation was performed following the procedure of Campbell et al. (2001), but the volatile elements Cu and Ga were added, because LA-ICP-MS analyses of these elements were made in the present study. The activity models of Wai and Wasson (1979) for Cu, Ga, and Au and Hultgren et al. (1973) for Pd were used, and the thermodynamic assessment of Chuang et al. (1986) was used for the activity of Ni. Other thermodynamic parameters were the same as in Campbell et al. (2001). The compositional trajectory followed by metal condensation from a solar gas is not a strong function of the total pressure, within the range thought to be appropriate to the solar nebula (Campbell et al., 2001). We assumed a nebular pressure of 10 Pa in this study, to facilitate comparison with previous work (Meibom et al.,

1999; 2000; 2001; Campbell et al., 2001; Petaev et al., 2001; 2003; Campbell and Humayun, 2004). In this calculation Fe is 5% condensed at 1370 K (19.0 wt% Ni in alloy) and 95% condensed at 1258 K (5.6 wt% Ni in alloy). The siderophile elements considered in this study are largely insensitive to oxidation under the range of conditions considered, and therefore there is an almost perfect trade-off in the condensation calculations between the assumed pressure and the dust/gas ratio. For example, the condensation temperatures for a 10 Pa gas of solar composition are the same as those of a 1 Pa gas with a dust/gas ratio of 10, or a 0.1 Pa gas with a dust/gas ratio of 100.

Palladium abundances do not vary much during equilibrium condensation of metal in a solar gas, because Pd and Fe have very similar volatilities in these circumstances. Therefore, the Pd-Ni trajectory in Fig. 6 is critical for genetic interpretation; the fact that it lies along the condensation trend, with only a slightly positive slope, strongly implicates volatility-based processes such as condensation and/or evaporation as responsible for the compositional variation seen within the grains (Campbell et al., 2001). If the zoning had been produced by any kind of redox-based process, the Pd/Ni ratios would have remained more constant because of the high siderophility of these two elements, Pd and Fe would have been fractionated by oxidation of Fe, and the Pd-Ni data would be chondritic and lie along the dotted line in Fig. 6. The same conclusion had been reached for zoned metal in the CB_b chondrite QUE 94411 by Campbell et al. (2001) and for zoned metal in the CH chondrites by Campbell and Humayun (2004).

The Ru-Ni and Ir-Ni trends have positive slopes and lie slightly below the calculated condensation trajectories for a solar gas of 10 Pa total pressure (Figure 6). These data are very similar to the Ru-Ni and Ir-Ni trends that were observed previously in zoned metal in QUE 94411 (Campbell et al., 2001); those authors suggested that this may indicate either condensation at lower gas pressures, in which the PGE-Ni trends are slightly shifted, or earlier removal of ultrarefractory metal prior to formation of the cores. Further detailed

modelling of refractory trace elements in the condensation+diffusion process is needed to understand the zoning in these grains.

The addition of volatile elements to the data set is a significant advancement of the present study beyond that of Campbell et al. (2001), and these elements provide further constraint on the formation of the zoned metal grains in CB_b chondrites. The Cu/Ni, Ga/Ni, and Au/Ni ratios are below their chondritic values at all points within the zoned metal (Fig. 6), consistent with the refractory nature of these grains. Given the uncertainties both in the data and in the activity model used (Wai and Wasson, 1979), the agreement between the observed Cu, Ga, and Au values and the calculated condensation trajectory is satisfactory. Assuming that the observed volatile element abundances do correspond to a condensation trajectory, the comparison in Fig. 6 suggests that the activity coefficients for Cu used in this calculation may have been overestimated by a factor of ~5-8, and those for Ga may have been overestimated by a factor of ~2-3. This corresponds to differences of 3-5 kcal/mol for ΔH^{xs} from those given by Wai and Wasson (1979).

The maximum Au values indicate that none of the zoned grains analyzed in this study record effective condensation temperatures below ~1260 K, at the reference nebular pressure of 10 Pa. The refractory element compositions correspondingly imply a maximum T_c of 1345 K to 1365 K for each of the zoned grains. Over the 1365 K to 1260 K interval in which the zoned metal apparently formed, Fe is calculated to be 22% to 95% condensed in a solar gas at 10 Pa total pressure.

Unzoned Metal Grains

Weisberg et al. (2001) showed that there is a strong positive correlation between Ni and Co in the unzoned metal from the CB_b chondrites QUE 94411 and HH 237. As discussed by those authors, this implies that the metal is primitive and undisturbed by thermal metamorphism, and is consistent with formation under nebular conditions, but could also have been the product of high-temperature oxidation/reduction reactions (e.g., Zanda et

al., 1994). Trace elemental analysis of the unzoned metal (Fig. 3) can help resolve between those two possibilities. As mentioned above, the Pd content of meteoritic metal is a sensitive indicator of redox versus volatility-controlled processing, because Pd has volatility similar to Fe but is more strongly siderophile. The Pd-Ni trend for unzoned metal in HH 237 and QUE 94627 lies much more closely to the calculated condensation trend, for a solar gas at 10 Pa, than it does to a constant Pd/Ni ratio. Furthermore, the trends in this metal between Ni and the volatile elements Cu, Ga, and Au all lie approximately parallel to the condensation trajectory, but the Au/Ni ratios are not at all constant, as would be expected from the ratio between these two siderophile elements during oxidation/reduction reactions. The three volatile elements are strongly correlated with one another (Fig. 4), despite the difference in chemical affinities between the siderophile Au, the chalcophile Cu, and the moderately lithophile Ga. These trace element data strongly support the notion that the composition of unzoned metal in CB_b chondrites was primarily established by a volatility-controlled process, such as condensation or evaporation in the solar nebula, and not by redox processing or by low-temperature metamorphism. The unzoned metal compositions suggest a maximum apparent T_c of ~1350 K, for grain #hh18a, and the S-rich unzoned metal grains all have apparent T_c below 1260 K, based on Ni and Au abundances. A lower limit on apparent T_c for the unzoned grains is not precisely fixed but is probably around 1100 K, neglecting grain #que58a, which contains Cu and Au at levels above those predicted along the condensation trajectory.

The refractory siderophile elements Ru and Ir are not as well-behaved as the volatile siderophiles in the unzoned metal from CB_b chondrites. Although Ru and Ir correlate very strongly with one another (Fig. 5a), they show no consistent pattern with either Ni (Fig. 3) or with the volatile siderophiles (represented by Au in Fig. 5b). A similar distribution was observed among the unzoned metal in the CH chondrites (Campbell and Humayun, 2004). Many of the unzoned metal grains (Figure 3) fall in the compositional range spanned within the zoned CB_b metal (Figure 6). These may or may not represent metal that was originally

zoned but that homogenized and/or that continued to equilibrate with the gas at lower temperatures. Other unzoned metal grains have significant refractory element depletions and cannot be a homogenized form of the zoned metal. Depletions in Ru and in Ir always occur together (Figures 3 and 5a), and are not correlated with Ni (Figure 3) or with Au (Figure 5b), which indicates that these grains condensed from gas reservoirs that had been variably depleted in refractory siderophiles. Similar refractory depletions were sometimes observed in CH metal by Campbell and Humayun (2004), who further suggested that the zoned metal itself may act as one, but perhaps not the only, refractory material that was sequestered from the gas.

Distinct differences exist between the trace element patterns of CB_b unzoned metal and those observed in the CB_a chondrites Bencubbin, Gujba, and Weatherford. As illustrated in Figure 3, correlations between the PGEs and Ni are well defined in CB_a metal, and reach higher trace PGE concentrations than those predicted by nebular condensation (Campbell et al., 2002). These strong correlations and high concentrations of PGEs are not generally observed in the CB_b unzoned metal (Figure 3), indicating different origins of the metal in the two different meteorite subgroups. An origin in a non-nebular, high temperature setting, such as an impact plume, has been advanced for the metal in CB_a chondrites (Kallemeyn et al., 2001; Campbell et al., 2002; Rubin et al., 2003). The large sulfide-rich metal nodules in the CB_b chondrites, which have textures and major element chemistries similar to metal in the CB_a chondrites, have not yet been analyzed for trace element concentrations; these may be important in deciphering the relationship between the CB chondrite subgroups.

Nebular Origin of Zoned and Unzoned Metal in CB_b Chondrites

In this section, we consider the hypothesis that the zoned and unzoned metal both condensed from a nebular gas, cooling by opacity reduction (e.g., Humayun and Cassen, 2000; Cassen, 2001). It should be noted that similar conditions may be encountered in

impact-generated vapor plumes (e.g. Campbell et al., 2002), and the possibility that all of the metal in both CB_a and CB_b chondrites formed from an impact plume, produced during a collision between planetesimal-size bodies, cannot be completely ruled out. Conditions in impact-produced vapor plumes are poorly constrained, but may conceivably generate the wide range of conditions recorded in the zoned and unzoned metal in CB_b chondrites as well as the large metal nodules in the CB_a chondrites. This hypothesis implies that the consistency between canonical nebular conditions and the gas densities that can produce the observed elemental distributions in the zoned metal is simply coincidental. Here, we discuss the formation of CB_b metal under the standard interpretation, that the gas from which it condensed was the solar nebula (Campbell et al., 2001; Krot et al., 2001; 2002; Lauretta et al., 2005; Meibom et al., 2001; Petaev et al., 2001; Weisberg et al., 2001).

The relationship between zoned and unzoned metal in the CB_b chondrites appears to be the same as that in the CH chondrites, as described by Campbell and Humayun (2004). Transient heating/cooling cycles in the nebula are required, in which the cooling rate is greater at high temperatures, when the zoned metal is forming (1365 K to 1260 K), than at lower temperatures, when the unzoned metal is condensing (1350 K to ~1100 K). Note that there is significant overlap in the apparent T_c ranges for zoned metal and S-poor unzoned metal, and it is possible that some, but not all, of the unzoned metal is diffusively homogenized zoned metal (Campbell and Humayun, 2004). The mechanism by which the high-T_c grains are rapidly removed and prevented from further equilibration with the hot solar nebula remains elusive; this problem persists for components of other meteorites as well (Campbell and Humayun, 2004).

The requirement of a faster cooling rate at higher nebular temperatures follows from the zoned metal having more refractory compositions, on average, than the unzoned metal, and from the fact that shorter timescales are necessary to prevent compositional zoning from being erased by diffusion. This change in cooling rate is also plausible in the context of the optical opacity of the locally condensing nebula. The opacity must increase greatly as the

major fraction of solids condenses (olivine has a condensation temperature similar to that of Fe-Ni metal (Grossman, 1972)), and this will reduce radiative heat loss and slow the cooling rate of the gas (Morfill, 1988; Boss, 1998; Humayun and Cassen, 2000; Cassen, 2001). The models of Petaev et al. (2003) for growth of zoned CH metal invoke cooling rates that increase with decreasing temperature; while this cannot be strictly excluded, it violates the expectation of a nebula that is thermally regulated by its opacity.

The duration for which the unzoned metal remained in the gas must have been sufficient to allow diffusive equilibration throughout the grain. Righter et al. (2005) have obtained diffusivity data for trace siderophile elements in Fe-Ni alloys. The slowest-diffusing element of those considered here is Ir, which has a diffusion coefficient (D) of $\sim 1.4 \times 10^{-16}$ m^2/s at 1250 K, which is a typical T_c value for the unzoned metal (at 10 Pa nebular pressure). At this temperature it would therefore take ~4 yr for the Ir distribution to homogenize in a metal grain of ~400 μm diameter. This is much longer than the days to weeks timescale that has been estimated for growth of zoned metal grains in CH and CB_b chondrites (Meibom et al., 1999; 2001; Campbell et al., 2001; Petaev et al., 2001; 2003; Campbell and Humayun, 2004). The diffusivity of Ir, being much lower than that of Ni, places a much stronger constraint on the minimum timescale for the unzoned grains to have formed. Furthermore, earlier comparisons of the rates of diffusion versus condensation of the zoned metal grains were generally based on D(Ni) (e.g., Campbell et al., 2001), and when one considers instead the slower diffusion of Ir, then it appears increasingly likely that condensation from a supersaturated gas played an important role in the zoned trace element profiles.

There is a small shift of the Cu, Ga, and Au data toward higher Ni contents than the metal condensation curve in Fig. 3, and also in the Ru and Ir abundances in Fig. 6. It is possible that this indicates the loss of a small fraction of Fe to associated silicate phases, but under the necessary mildly oxidizing conditions, one would expect Ga to be more depleted than is observed. Alternatively, Weisberg et al. (2001) reported bulk Fe/Ni depletions,

relative to CI abundances, in QUE 94411, and the shift to higher Ni seen in Figs. 3 and 6 may therefore be related to a non-chondritic Fe/Ni ratio in the gas in which the CB_b metal condensed.

It is apparent from the contrast between the bulk compositions of unzoned metal plotted in Fig. 3 and the compositions in zoned metal displayed in Fig. 6 that not all of the unzoned metal can be simply a homogenized form of the zoned metal. This is uniformly true for the S-rich metal grains, which are volatile depleted but nonetheless all have Cu, Ga, and Au abundances that generally exceed those observed in the zoned metal. The Cu contents found in the S-rich unzoned metal range from 8 to 225 ppm, but are <6 ppm in the zoned metal interiors. Likewise, the minimum Ga and Au abundances in the S-rich unzoned metal (0.56 ppm and 0.23 ppm, respectively) are similar to the maximum values in the zoned metal (0.64 ppm and 0.20 ppm, respectively). The compositions of the S-poor, unzoned metal have some similarities to the zoned metal (Figs. 3 and 6), and several of those grains have compositions that are consistent with homogenization of a zoned grain. However, even some of the S-poor unzoned grains are distinctly refractory-poor (e.g., #hh39e and #que58a) and/or have higher volatile abundances (e.g., #que59c), and therefore cannot be simply homogenized zoned grains (although it is not impossible that a grain like #que59c, which is not refractory-depleted, could once have been a zoned grain that gained volatiles during re-equilibration with the gas at lower temperature). These observations suggest that the unzoned metal grains were produced at lower temperatures, on average, than the zoned metal that is found in the same meteorites, although there is significant overlap in the temperature ranges recorded in the two metal populations. Diffusive equilibration requires that the unzoned metal must have resided in the hot nebula for a much longer period than the zoned metal. The same conclusion was reached by Campbell and Humayun (2004) with regard to zoned and unzoned metal in CH chondrites.

Several of the CB_b metal grains, both zoned and unzoned, have higher concentrations of Cu and/or Ga at the outermost rims than in the grain interiors (Figure 2).

These enrichments in Cu are much lower than those observed in CH chondrites, and are observed only on those grains that have interior Cu contents that are low, below ~20 ppm. It is probable that this indicates that Cu has diffused into the metal from the surrounding environment. This could have happened on the CB_b parent body; the much smaller degree of Cu diffusion is consistent with the conclusions above that the CB_b metal experienced less thermal metamorphism than the CH metal did (Campbell and Humayun, 2004). However, because of the very limited degree of observed diffusion, and because both Cu and Ga have higher diffusion coefficients than the refractory elements (e.g., Righter et al., 2005), it is also possible that this could be a nebular signature, in which a minor amount of volatile elements diffused into the grains during cooling of the surrounding nebular gas. Using again the diffusion coefficients of Righter et al. (2005), which were measured from natural compositions, we estimate that this level of diffusion of Cu at 1100 K would have required ~10 days to have diffused from a surrounding nebula. This residence time would not significantly disturb the distribution of more refractory elements such as Ni or Ir. Again, more detailed modeling of the condensation+diffusion processes in these grains is warranted.

Campbell and Humayun (2004), in their LA-ICP-MS study of metal in CH chondrites, reported much higher Cu abundances in the zoned metal of those meteorites; the maximum Cu content reported for zoned metal in that study was 374 ppm, much higher than in the present data (14 ppm; Appendix), and Cu values in excess of 10 ppm were common in the earlier study, even extending 50 μm or more into the zoned metal grains. Campbell and Humayun (2004) concluded that the Cu distributions in zoned metal from CH chondrites were the product of thermal metamorphism, probably on the parent body, in which Cu diffused into the metal from the surrounding environment. The observed frequency of taenite decomposition in those meteorites further supported a scenario of significant parent body metamorphism. In contrast to those observations from the CH chondrites, the zoned metal from the CB_b chondrites have low Cu contents approximately

consistent with nebular processing (Fig. 6), and no indication of Cu diffusion far into the interior of the grains (Fig. 2; Appendix). This is consistent with the observation that taenite decomposition is much less common in CB_b metal than it is in CH metal. The Cu distributions in zoned metal in CB_b chondrites are further evidence that these meteorites are among the most primitive known, and have been subjected to minimal low-temperature metamorphism (Weisberg et al., 2001; Krot, 2002).

We also note that the frequency of zoned metal observed in the CB_b chondrites in this study (60% to 70%) is significantly higher than that which had been reported earlier. The estimate of 15% zoned metal grains, made by Meibom et al. (2001), appears to have been based on a count of grains in a Ni K_α map. This procedure can be expected to identify only those grains with most extreme zoning, and highest central Ni contents, and thereby underrepresent the frequency of zoned metal grains. As noted by Meibom et al. (2001), the high rate of occurrence of zoned metal grains can be used as a constraint on nebular models for their formation. For example, a model proposed by Meibom et al. (2000), involving transport of metal grains from hot to cool regions by turbulent diffusion, predicted a zoned metal fraction of ~0.5%. An accurate model of the nebular setting in which the CB_b and CH metal formed is required by the present results to involve cooling rates that decrease with decreasing temperature and sub-equal numbers of zoned and unzoned grains.

The Presence of Sulfide Inclusions in CB_b Unzoned Metal

The origin of the sulfide inclusions in some of the unzoned metal remains perplexing. The trace element compositions of the S-rich grains lie along the trend described by the S-poor grains, implying similar volatility-based origins; there is no suggestion in these data of mixing between an S-rich component and other, S-poor metal. The fact that the S-rich grains are concentrated at the low-Ni end of this trend is consistent with S being a volatile element. However, the calculated condensation temperature of troilite in a solar gas composition is ~700 K (Grossman, 1972; Lauretta et al., 1996), which is

significantly lower than the ~1100 K limit that we have estimated on the basis of the volatile siderophile elements in CB_b unzoned metal.

The kinetics of sulfidation of metal are fast relative to nebular timescales (Lauretta et al., 1996; 1998), and it is possible that sulfidation took place at low temperatures after the trace element composition of the metal had been established. In this scenario, the trace element distributions were locked in by the sluggish diffusion rates of siderophile elements in metal (Righter et al., 2005). However, there are textural features of the S-rich metal that are inconsistent with corrosion of the metal grains by an S-rich gas. Experimental studies of kamacite sulfidation (Lauretta et al., 1996; 1998) and petrographic examinations of sulfidized metal in primitive ordinary chondrites (Lauretta et al., 2001) both indicate that corrosion forms an outer shell of sulfide around the grain that is unlike the distribution of sulfide inclusions observed in the unzoned CB_b metal (Figure 1). Also, there is no obvious reason for this mechanism to preferentially cause sulfidation of the low-Ni unzoned metal over high-Ni metal, as is observed (Figure 3).

The occurrence of sulfides within the metal grains, rather than on their outer surfaces, suggests that the sulfide may have co-formed with the metal, or that the sulfide precipitated from a metal- and S-rich phase, such as a melt. Grain hh10a in Figure 1 is a particularly striking example of the heterogeneous distribution of sulfides that can be encountered in unzoned CB_b metal. Based strictly on textural observations such as this, one might postulate that these grains were once partially molten metal sulfide objects that solidified and annealed, forming sulfide-rich and sulfide-poor domains such as those observed in grain hh10a (Figure 1). However, the eutectic temperature in the Fe-FeS system is 1261 K, which, although low, is far above the condensation point for sulfur in a gas of solar composition (710 K; Lauretta et al., 2001). Any partially molten iron-sulfide object would have very rapidly lost its S by devolatilization to the surrounding gas. Furthermore, our measurements provide no support for elemental fractionations between sulfide-rich and

sulfide-poor regions of the metal grains, which should have been expected from metal-melt partitioning.

Lauretta et al. (2001) have noted that, although the condensation point of troilite is effectively independent of the assumed nebular pressure for a fixed gas composition, it is sensitive to variations in the H_2S/H_2 ratio, such as those imposed by elevating the dust/gas ratio. A dust/gas ratio of 100, for example, raises the condensation point of troilite in a 10 Pa nebula to 1150 K (Lauretta et al., 2001). However, the elevated dust/gas ratio also increases the partial pressures of siderophile elements, and our estimate of the lower bound of temperature recorded by the volatile siderophiles in the unzoned CB_b metal likewise increases, from ~1100 K to ~1300 K with a dust/gas ratio of 100. Further increasing the dust/gas ratio has less impact on the T_c of troilite because of changes in the speciation of S-bearing gases (Lauretta et al., 2001). Comparing the troilite condensation calculations of Lauretta et al. (2001) with our metal alloy condensation calculations, we can find no circumstances under which troilite is stable at a temperature high enough to satisfy the constraints placed by the depletion of volatile siderophiles in the unzoned CB_b metal.

It is likely that the origin of the sulfide inclusions in the CB_b metal would provide an important further constraint on the history of these meteorites and their components. Further study of the unzoned metal, including a wider range of trace elements, would be useful for confirming (or disproving) that the S-rich grains are part of the same population as the S-poor grains. In addition, a similar study of the large metal-sulfide aggregates described by Weisberg et al. (2001) could establish the relationship between those objects and the sulfide-bearing unzoned metal studied here. Finally, Weisberg et al. (2001) noted that the troilites in the CB_b metal are Cr-bearing, 2.0-2.5 wt% on average. Detailed examination of the relationship between the compositions of troilite inclusions and their associated metal grains may be informative. It is also possible that compositional effects on the free energy of Cr-bearing troilite may significantly affect its condensation temperature

relative to that of the pure FeS phase considered by Lauretta et al. (2001); this remains to be evaluated.

CONCLUSIONS

The zoned metal in CB_b chondrites formed by condensation under conditions similar to those of the canonical solar nebula. Comparison of the refractory element enrichments in the zoned grain cores, and the volatile element depletions throughout the grains, to equilibrium condensation calculations suggests a range of apparent condensation temperatures between 1365 K and 1260 K, at an assumed total pressure of 10 Pa. The effect of diffusion of trace elements on the zoning patterns, and the corresponding apparent condensation temperatures, has not been fully evaluated.

The trace element compositions of unzoned CB_b metal are also consistent with a nebular origin. The volatile element abundances in the unzoned grains are well correlated with one another, despite differences in chemistry aside from their shared volatility. These metal grains formed from gas parcels that were variably depleted in refractory elements. Unzoned metal that contains sulfide inclusions formed at temperatures (1260 K to ~1100 K) lower than the temperature range in which the zoned metal formed, and has higher volatile element abundances. The presence of sulfide in these grains is not fully understood. Sulfide-free unzoned metal appears to record condensation temperatures that overlap those of both the zoned and unzoned grains; some, but not all, of this metal may have been produced by diffusive equilibration of metal that was previously zoned.

In addition to their coexistence in the CB_b meteorites, the apparent complementarity between the highly volatile-depleted, refractory-rich zoned metal and the less volatile-depleted, frequently refractory-depleted unzoned metal supports a linked origin for these two populations. This origin appears to be very similar to that of zoned and unzoned metal in CH chondrites (Campbell and Humayun, 2004), and involves transient heating/cooling cycles, with high cooling rates that decrease with decreasing temperature. Relative to CH metal, the CB_b metal has fewer instances of plessitic decomposition of taenite and much less diffuse penetration of Cu. This lack of thermal metamorphism underscores the highly

primitive nature of the CB_b chondrites, which appear to be among the most pristine meteoritic materials and preserve extensive clues to their nebular origin.

Acknowledgments–We are grateful to the Meteorite Working Group and to the American Museum of Natural History for the meteorite sections. The manuscript was improved by the input from reviewers H. Newsom, A. Krot, and R. Korotev. This work was supported by NASA through grants NAG5-13133 to M. H. and NAG5-11546 to M. K. W.

REFERENCES

Anders E. and Grevesse N. 1989. Abundances of the elements: Meteoritic and solar. *Geochimica et Cosmochimica Acta* **53**, 197-214.

Boss A. P. 1998. Temperatures in protoplanetary disks. *Annual Reviews of Earth & Planetary Science* **26**, 53-80.

Campbell A. J. and Humayun M. 1999. Trace element microanalysis in iron meteorites by laser ablation ICPMS. *Anaytical Chemistry* **71**, 939-946.

Campbell A. J. and Humayun M. 2004. Formation of metal in the CH chondrites ALH 85085 and PCA 91467. *Geochimica et Cosmochimica Acta* **68**, 3409-3422.

Campbell A. J., Humayun M., and Weisberg M. K. 2000. Siderophile element distributions in zoned metal grains in Hammadah al Hamra 237. *Meteoritics & Planetary Science* **35**, A38-A39.

Campbell A. J., Humayun M., Meibom A., Krot A. N., and Keil K. 2001. Origin of zoned metal grains in the QUE94411 chondrite. *Geochimica et Cosmochimica Acta* **65**, 163-180.

Campbell A. J., Humayun M., and Weisberg M. K. 2002. Siderophile element constraints on the formation of metal in the metal-rich chondrites Bencubbin, Weatherford, and Gujba. *Geochimica et Cosmochimica Acta* **66**, 647-660.

Campbell A. J., Simon S. B., Humayun M. and Grossman L. 2003. Chemical evolution of metal in refractory inclusions in CV3 chondrites. *Geochimica et Cosmochimica Acta* **67**, 3119-3134.

Cassen P. 2001. Nebular thermal evolution and the properties of primitive planetary materials. *Meteoritics & Planetary Science* **36**, 671-700.

Chuang Y.-Y., Hsieh K.-C., and Chang Y. A. 1986. A thermodynamic analysis of the phase equilibria of the Fe-Ni system above 1200 K. *Metallurgical Transactions A* **17A**, 1373-1380.

Grossman L. 1972. Condensation in the primitive solar nebula. *Geochimica et Cosmochimica Acta* **36**, 597-619.

Grossman L. and Olsen E. 1974. Origin of the high-temperature fraction of C2 chondrites. *Geochimica et Cosmochimica Acta* **38**, 173-187.

Grossman L., Olsen E., and Lattimer J. M. 1979. Silicon in carbonaceous chondrite metal: Relic of high-temperature condensation. *Science* **206**, 449-451.

Hezel D. C., Palme H., Brenker F., and Nasdala L. 2003. Evidence for fractional condensation and reprocessing at high temperatures in CH chondrites. *Meteoritics & Planetary Science* **38**, 1199-1215.

Hultgren R., Desai P. D., Hawkins D. T., Gleiser M., and Kelley K. K. 1973. *Selected Values of the Thermodynamic Properties of Binary Alloys*. American Society for Metals.

Humayun M. and Cassen P. 2000. Processes determining the volatile abundances of the meteorites and terrestrial planets. In *Origin of the Earth and Moon* (eds. R. M. Canup and K. Righter). University of Arizona Press, Tucson, pp. 3-23.

Humayun M., Campbell A. J., Zanda B., and Bourot-Denise M. 2002. Formation of Renazzo chondrule metal inferred from siderophile elements (abstract #1965). 33rd Lunar and Planetary Science Conference. CD-ROM.

Kallemeyn G. W., Rubin A. E., and Wasson J. T. (2001) Compositional studies of Bencubbin dark silicate host and an OC clast: Relationships to other meteorites and implications for their origin (abstract #2070). 32nd Lunar and Planetary Science Conference. CD-ROM.

Kelly W. R. and Larimer J. W. 1977. Chemical fractionations in meteorites – VIII. Iron meteorites and the cosmochemical history of the metal phase. *Geochimica et Cosmochimica Acta* **41**, 93-111.

Krot A. N., Meibom A., Russell S. S., Alexander C. M. O'D., Jeffries T. E., and Keil K. 2001. A new astrophysical setting for chondrule formation. *Science* **291**, 1776-1779.

Krot A. N., Meibom A., Weisberg M. K., and Keil K. 2002. The CR chondrite clan: Implications for early solar system processes. *Meteoritics & Planetary Science* **37**, 1451-1490.

Lauretta D. S., Kremser D. T., and Fegley B. Jr. 1996. The rate of iron sulfide formation in the solar nebula. *Icarus* **122**, 288-315.

Lauretta D. S., Lodders K., and Fegley B. Jr. 1998. Kamacite sulfurization in the solar nebula. *Meteoritics & Planetary Science* **33**, 821-833.

Lauretta D. S., Buseck P. R., and Zega T. J. 2001. Opaque minerals in the matrix of the Bishunpur (LL3.1) chondrite: Constraints on the chondrule formation environment. *Geochimica et Cosmochimica Acta* **65**, 1337-1353.

Lauretta D. S., Guan Y., and Leshin L. A. 2005. Hydrogen abundances in metal grains form the Hammadah al Hamra (HaH) 237 metal-rich chondrite: A test of the nebular-formation theory (abstract #1839). 36th Lunar and Planetary Science Conference. CD-ROM.

Mehrer H. 1990. Diffusion in solid metals and alloys. In *Landolt-Börnstein Numerical Data and Functional Relationships in Science and Technology, Group III, Volume 26* (ed. O. Madelung). Springer-Verlag, Heidelberg.

Meibom A., Petaev M. I., Krot A. N., Wood J. A., and Keil K. 1999. Primitive FeNi metal grains in CH carbonaceous chondrites formed by condensation from a gas of solar composition. *Journal of Geophysical Research* **104**, 22053-22059.

Meibom A., Desch S. J., Krot A. N., Cuzzi J. N., Petaev M. I., Wilson L., and Keil K. 2000. Large scale thermal events in the solar nebula recorded in Fe, Ni metal condensates in primitive meteorites. *Science* **288**, 839-841.

Meibom A., Petaev M. I., Krot A. N., Keil K., and Wood J. A. 2001. Growth mechanism and additional constraints on FeNi metal condensation in the solar nebula. *Journal of Geophysical Research* **106**, 32797-32801.

Morfill G. E. 1988. Protoplanetary accretion disks with coagulation and evaporation. *Icarus* **75**, 371-379.

Petaev M. I., Meibom A., Krot A. N., Wood J. A., and Keil K. 2001. The condensation origin of zoned metal grains in Queen Alexandra Range 94411: Implications for the formation of the Bencubbin-like chondrites. *Meteoritics & Planetary Science* **36**, 93-106.

Petaev M. I., Wood J. A., Meibom A., Krot A. N., and Keil K. 2003. The ZONMET thermodynamic and kinetic model of metal condensation. *Geochimica et Cosmochimica Acta* **67**, 1737-1751.

Righter K., Campbell A. J., Humayun M., and Hervig R. L. 2004. Partitioning of Ru, Rh, Pd, Re, Ir, and Au between Cr-bearing spinel, olivine, pyroxene and silicate melts. *Geochimica et Cosmochimica Acta* **68**, 867-880.

Righter K., Campbell A. J., and Humayun M. 2005. Diffusion of siderophile elements in Fe metal: Application to zoned metal grains in chondrites. *Geochimica et Cosmochimica Acta*, in press.

Rubin A. E., Kallemeyn G. W., Wasson J. T., Clayton R. N., Mayeda T. K., Grady M., Verchovsky A. B., Eugster O., and Lorenzetti L. 2003. Formation of metal and silicate globules in Gujba: A new Bencubbin-like meteorite fall. *Geochimica et Cosmochimica Acta* **67**, 3283-3298.

Wai C. M. and Wasson J. T. 1979. Nebular condensation of Ga, Ge and Sb and the chemical classification of iron meteorites. *Nature* **282**, 790-793.

Wasson J. T., Ouyang X., Wang J. and Jerde E. 1989. Chemical classification of iron meteorites: XI. Multi-element studies of 38 new irons and the high abundance of ungrouped irons from Antarctica. *Geochimica et Cosmochimica Acta* **53**, 735-744.

Weisberg M. K., Prinz M., Clayton R. N., Mayeda T. K., Grady M. M., and Pillinger C. T. 1995. The CR chondrite clan. *Proceedings of the NIPR Symposium on Antarctic Meteorites* **8**, 11-32.

Weisberg M. K., Prinz M., Clayton R. N., Mayeda T. K., Sugiura N., Zashu S., and Ebihara M. 1999. QUE94411 and the origin of bencubbinites (abstract #1416). 30th Lunar and Planetary Science Conference. CD-ROM.

Weisberg M. K., Prinz M., Clayton R. N., Mayeda T. K., Sugiura N., Zashu S., and Ebihara M. 2001. A new metal-rich chondrite grouplet. *Meteoritics & Planetary Science* **36**, 401-418.

Wood J. A. and Morfill G. E. 1988. A review of solar nebula models. In *Meteorites and the Early Solar System* (eds. J. F. Kerridge and M. S. Matthews). University of Arizona Press, Tucson, pp. 329-347.

Zanda B., Bourot-Denise M., Perron C., and Hewins R. H. 1994. Origin and metamorphic redistribution of silicon, chromium, and phosphorus in the metal of chondrites. *Science* **265**, 1846-1849.

Zanda B., Bourot-Denise M., Hewins R., Cohen B. A., Delaney J. S., Humayun M., and Campbell A. J. 2002. Accretion textures, iron evaporation and re-condensation in Renazzo chondrules (abstract #1852). 33rd Lunar and Planetary Science Conference. CD-ROM.

Table 1. Laser ablation ICP-MS analyses of unzoned metal grains in HH 237 and QUE 94627. Data are means and 1σ standard errors, and are in ppm unless otherwise noted. Italicized entries without uncertainties are detection limits only.

grain #		Fe wt%	Ni wt%	Cu	Ga	Ru	Pd	Ir	Au
hh10a	S-rich	92.9 ± 0.2	7.06 ± 0.16	45.1 ± 1.5	1.21 ± 0.05	5.08 ± 0.12	3.16 ± 0.09	3.31 ± 0.08	0.341 ± 0.015
hh10f	S-poor	93.0 ± 0.2	6.95 ± 0.15	8.1 ± 1.3	0.62 ± 0.10	5.31 ± 0.23	2.69 ± 0.11	3.07 ± 0.16	0.188 ± 0.015
hh11a	S-poor	93.5 ± 0.2	6.48 ± 0.16	36.5 ± 1.7	1.14 ± 0.04	3.98 ± 0.11	2.65 ± 0.08	2.56 ± 0.08	0.414 ± 0.014
hh12c	S-rich	93.7 ± 0.1	6.25 ± 0.15	80 ± 3	2.09 ± 0.08	3.89 ± 0.09	2.76 ± 0.07	2.39 ± 0.05	0.533 ± 0.016
hh12e	S-rich	93.3 ± 0.3	6.72 ± 0.27	15.4 ± 1.4	0.86 ± 0.07	3.15 ± 0.16	2.98 ± 0.08	2.31 ± 0.08	0.276 ± 0.020
hh13a	S-poor	93.1 ± 0.2	6.87 ± 0.19	9 ± 2	0.60 ± 0.06	4.22 ± 0.18	2.82 ± 0.07	2.64 ± 0.11	0.162 ± 0.012
hh14b	S-rich	93.5 ± 0.2	6.49 ± 0.22	41.0 ± 1.8	1.35 ± 0.05	3.22 ± 0.19	2.76 ± 0.10	2.20 ± 0.08	0.376 ± 0.023
hh14c	S-rich	93.8 ± 0.2	6.19 ± 0.16	27.5 ± 1.0	1.09 ± 0.06	3.45 ± 0.09	2.65 ± 0.09	2.26 ± 0.07	0.349 ± 0.016
hh15a	S-poor	91.7 ± 0.2	8.34 ± 0.22	6.1 ± 0.5	0.31 ± 0.05	4.80 ± 0.19	3.37 ± 0.13	2.68 ± 0.06	0.108 ± 0.020
hh15d	S-poor	90.2 ± 0.2	9.79 ± 0.19	4.2 ± 0.3	0.28 ± 0.06	4.68 ± 0.17	3.44 ± 0.12	2.91 ± 0.07	0.096 ± 0.018
hh17b	S-rich	94.1 ± 0.2	5.95 ± 0.16	8.1 ± 0.4	0.56 ± 0.06	3.47 ± 0.13	2.66 ± 0.10	2.25 ± 0.06	0.226 ± 0.018
hh18a	S-poor	89.3 ± 0.2	10.70 ± 0.16	2.15 ± 0.09	0.59 ± 0.04	7.72 ± 0.19	3.96 ± 0.09	4.26 ± 0.08	0.059 ± 0.006
hh35a	S-poor	89.6 ± 0.4	10.41 ± 0.35	7.3 ± 0.4	0.25 ± 0.06	4.62 ± 0.18	3.66 ± 0.16	2.92 ± 0.09	0.069 ± 0.012
hh35c	S-rich	92.8 ± 0.2	7.20 ± 0.22	105 ± 3	1.64 ± 0.08	0.65 ± 0.05	2.54 ± 0.11	0.50 ± 0.02	0.479 ± 0.015
hh36b	S-rich	93.1 ± 0.2	6.88 ± 0.19	225 ± 9	3.20 ± 0.17	3.30 ± 0.25	2.90 ± 0.09	2.42 ± 0.08	0.655 ± 0.026
hh36d	S-rich	93.7 ± 0.2	6.31 ± 0.20	17.8 ± 0.9	0.73 ± 0.05	2.76 ± 0.12	2.40 ± 0.10	1.92 ± 0.05	0.395 ± 0.014
hh37a	S-poor	91.4 ± 0.1	8.58 ± 0.15	3.7 ± 0.3	*0.16*	4.54 ± 0.11	3.42 ± 0.11	2.78 ± 0.07	0.144 ± 0.009
hh37c	S-poor	92.1 ± 0.2	7.86 ± 0.17	5.5 ± 0.2	0.34 ± 0.05	4.18 ± 0.11	3.09 ± 0.10	2.83 ± 0.06	0.200 ± 0.011
hh37d	S-poor	93.0 ± 0.2	6.97 ± 0.17	3.2 ± 0.5	0.31 ± 0.08	4.18 ± 0.19	2.84 ± 0.05	2.94 ± 0.10	0.097 ± 0.016
hh38c	S-poor	94.0 ± 0.3	6.03 ± 0.28	14 ± 6	0.40 ± 0.08	4.14 ± 0.45	3.08 ± 0.20	3.17 ± 0.27	0.152 ± 0.031
hh38e	S-poor	94.7 ± 0.2	5.34 ± 0.19	12 ± 5	*0.22*	3.92 ± 0.31	2.69 ± 0.11	2.63 ± 0.18	0.167 ± 0.048
hh39e	S-poor	93.3 ± 0.4	6.74 ± 0.36	113 ± 3	2.77 ± 0.13	0.79 ± 0.05	2.86 ± 0.15	0.30 ± 0.02	0.348 ± 0.031
hh40a	S-poor	91.7 ± 0.1	8.29 ± 0.11	2.3 ± 0.2	*0.26*	4.75 ± 0.15	3.21 ± 0.07	2.74 ± 0.06	0.084 ± 0.015
hh44a	S-poor	92.1 ± 0.3	7.85 ± 0.30	3.0 ± 0.5	*0.14*	4.85 ± 0.21	3.16 ± 0.18	2.79 ± 0.09	0.086 ± 0.021
hh44e	S-poor	91.6 ± 0.3	8.39 ± 0.26	4.6 ± 0.3	*0.14*	4.76 ± 0.14	3.22 ± 0.09	2.84 ± 0.10	0.136 ± 0.026
que57b	S-poor	92.6 ± 0.3	7.44 ± 0.28	14 ± 2	0.40 ± 0.05	5.77 ± 0.22	2.99 ± 0.17	4.03 ± 0.12	0.217 ± 0.025
que58a	S-poor	94.1 ± 0.3	5.93 ± 0.26	1300 ± 268	22 ± 7	0.13 ± 0.04	2.43 ± 0.14	0.04 ± 0.01	1.126 ± 0.085
que59c	S-rich	93.7 ± 0.1	6.25 ± 0.10	176 ± 11	2.70 ± 0.07	3.83 ± 0.15	2.70 ± 0.07	2.70 ± 0.09	0.525 ± 0.031
que60c	S-poor	93.6 ± 0.2	6.43 ± 0.19	97 ± 3	2.67 ± 0.14	3.57 ± 0.17	2.87 ± 0.16	2.35 ± 0.08	0.745 ± 0.043
que63c	S-rich	93.6 ± 0.1	6.45 ± 0.14	32 ± 2	1.13 ± 0.04	3.65 ± 0.15	2.73 ± 0.14	2.29 ± 0.08	0.324 ± 0.019

FIGURE CAPTIONS

Fig. 1. X-ray maps of Ni K_α (left) and S K_α (right) from HH 237. Zoned metal grains #hh10b and #hh10d, and unzoned metal grains #hh10a and #hh10f, are indicated. Sulfide inclusions are visible in #hh10a. Scale bars are 200 μm.

Fig. 2. LA-ICP-MS profiles across unzoned metal grains #hh35c and #que57b and zoned grain #hh11b.

Fig. 3. Trace element concentrations in unzoned metal grains, plotted against Ni. Circles: HH 237 metal; squares: QUE 94627 metal; open symbols: sulfide-poor metal; shaded symbols: sulfide-rich metal. Solid lines: equilibrium trajectory of metal alloy condensation from a solar gas at 10 Pa total pressure; dotted lines: chondritic ratio of each element pair (Anders and Grevesse, 1989); dotted ellipses: outline of data from CB_a metal (Campbell et al., 2002).

Fig. 4. Volatile siderophile elements in unzoned metal grains in HH 237 and QUE 94627: a) Cu and b) Ga plotted against Au. Symbols are the same as in Fig. 3. Data for Ga below the dashed line are upper limits only. The dotted lines indicate the chondritic ratio for each element pair.

Fig. 5. Siderophile elements in unzoned metal grains in HH 237 and QUE 94627: a) Ru and b) Au plotted against Ir. Symbols are the same as in Figs. 3 and 4. The dotted lines indicate the chondritic ratio for each element pair.

Fig. 6. Trace element concentrations in zoned metal grains, plotted against Ni. LA-ICP-MS measurements from within all 9 grains listed in Table EA1 are included (solid circles). Data

below detection limits are not shown. Solid lines: calculated equilibrium trajectory of metal alloy composition during condensation in a solar gas at 10 Pa; dotted lines: chondritic ratios of each element pair.

APPENDIX

Table A1. LA-ICP-MS profile measurements for zoned metal grains in HH 237 and QUE 94627.

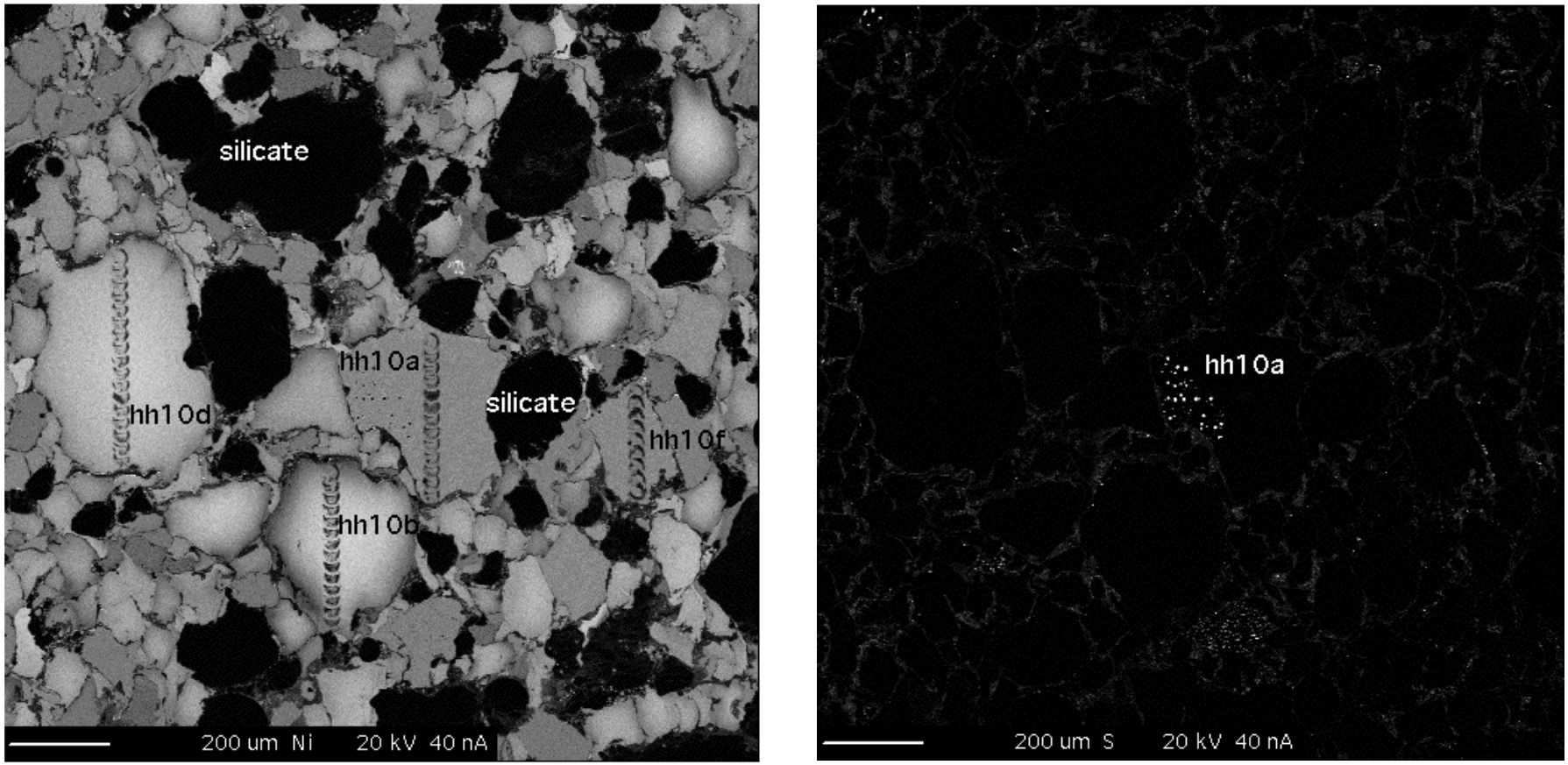
silicate
hh10a
hh10d
silicate
hh10f
hh10b
200 um Ni 20 kV 40 nA
hh10a
200 um S 20 kV 40 nA

Figure 1

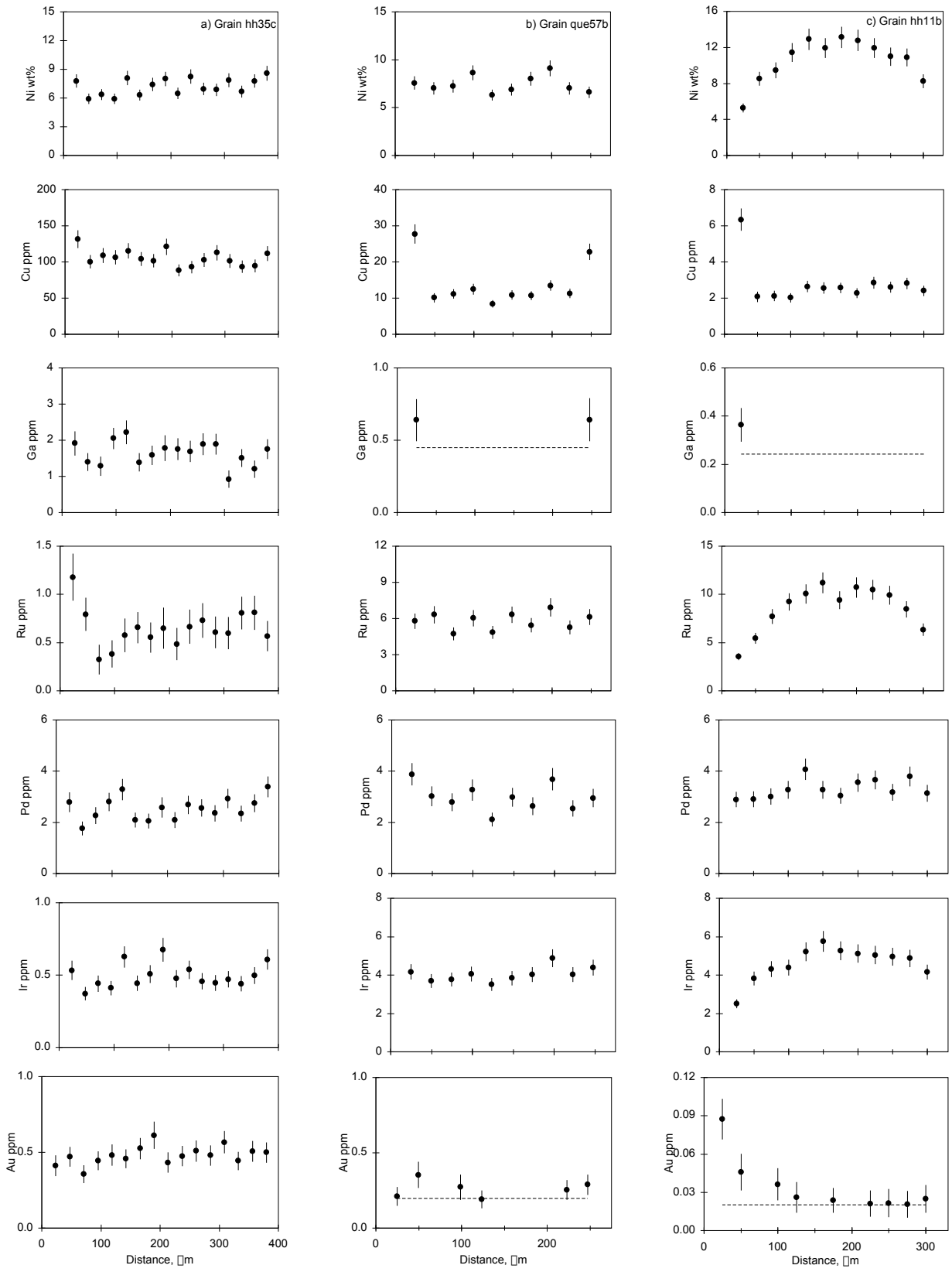
a) Grain hh35c
b) Grain que57b
c) Grain hh11b
Ni wt%
Cu ppm
Ga ppm
Ru ppm
Pd ppm
Ir ppm
Au ppm
Distance, □m

Figure 2

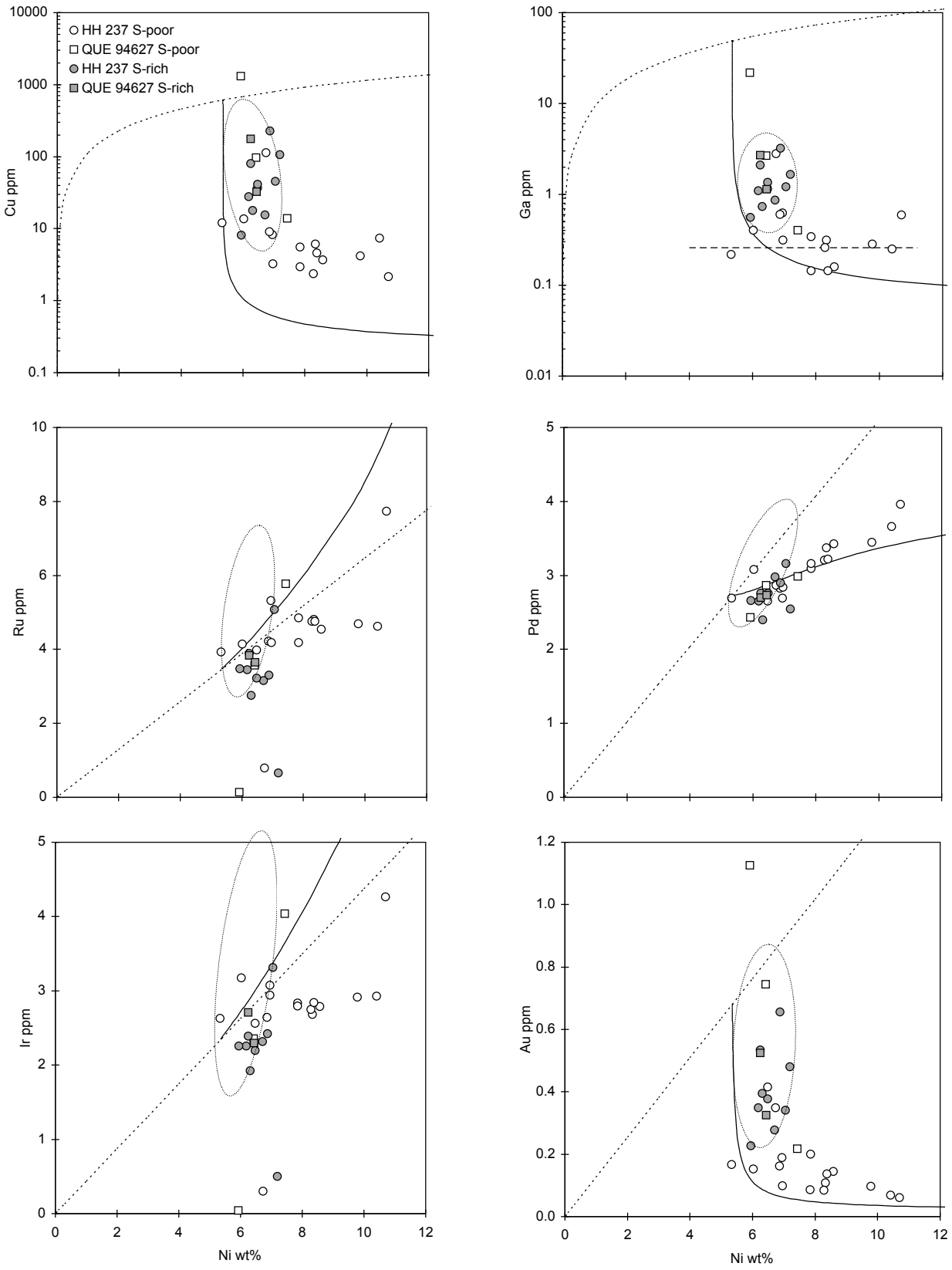
HH 237 S-poor
QUE 94627 S-poor
HH 237 S-rich
QUE 94627 S-rich
Cu ppm
Ga ppm
Ru ppm
Pd ppm
Ir ppm
Au ppm
Ni wt%
Ni wt%

Figure 3

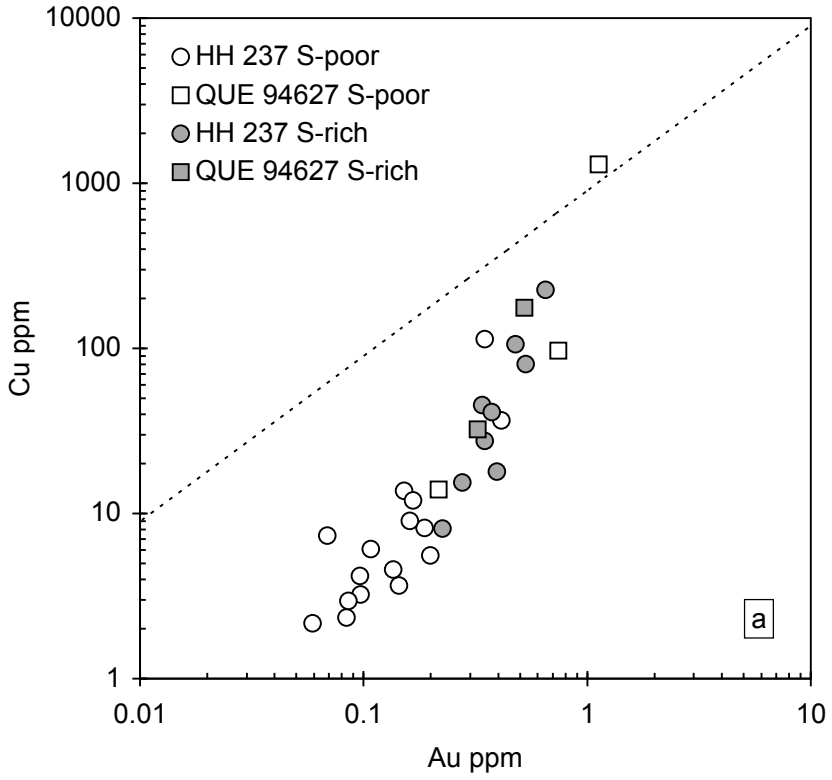
10000
1000
100
10
1
Cu ppm
HH 237 S-poor
QUE 94627 S-poor
HH 237 S-rich
QUE 94627 S-rich
a
0.01
0.1
1
10
Au ppm

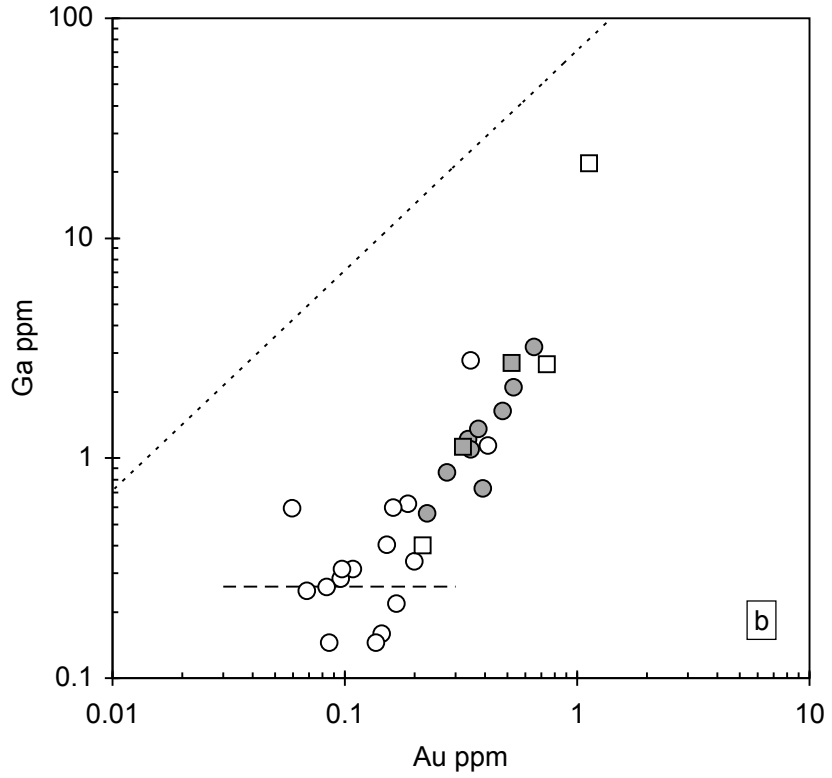
100
10
1
0.1
Ga ppm
b
0.01
0.1
1
10
Au ppm

Figure 4

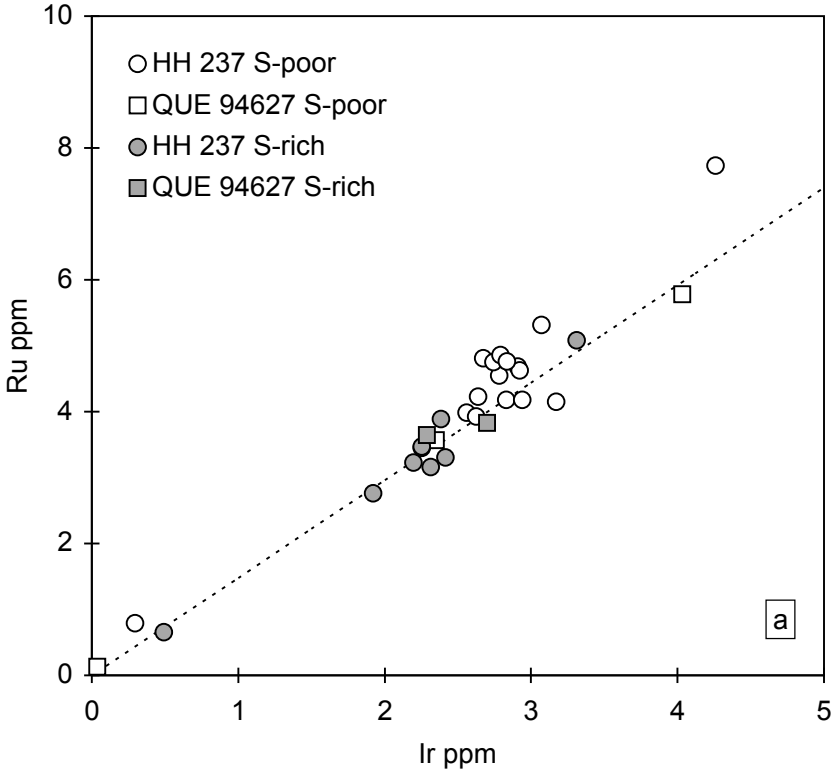
HH 237 S-poor
QUE 94627 S-poor
HH 237 S-rich
QUE 94627 S-rich
Ru ppm
Ir ppm
a
0
2
4
6
8
10
0
1
2
3
4
5

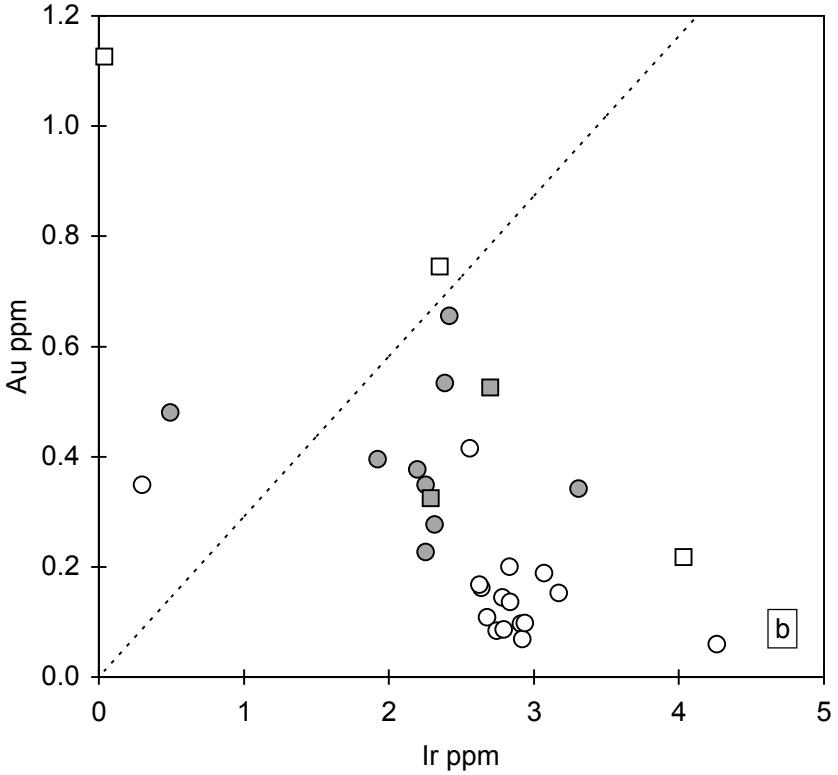
Au ppm
Ir ppm
b
0.0
0.2
0.4
0.6
0.8
1.0
1.2
0
1
2
3
4
5

Figure 5

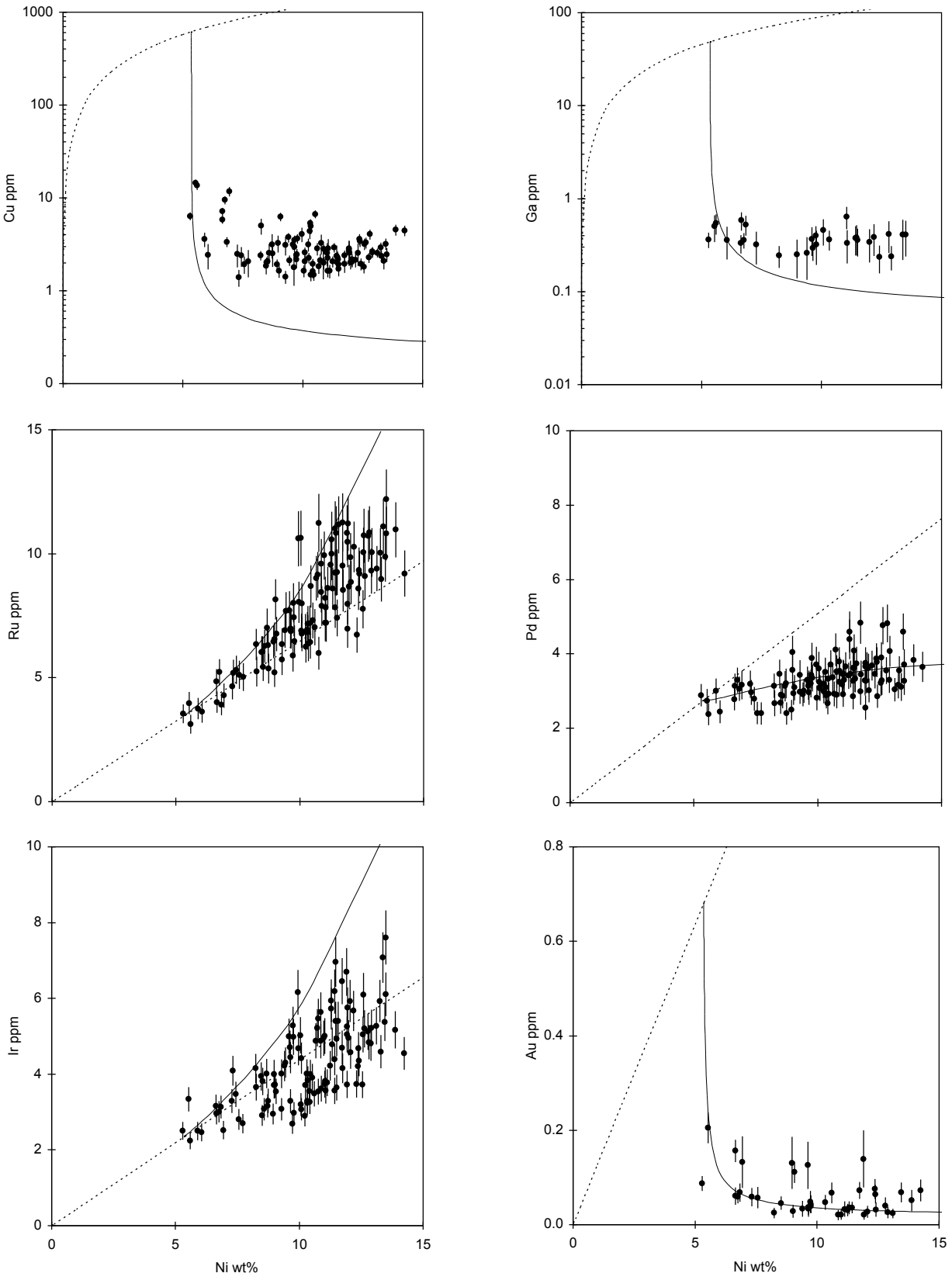
Cu ppm
1000
100
10
1
0
Ga ppm
100
10
1
0.1
0.01
Ru ppm
15
10
5
0
Pd ppm
10
8
6
4
2
0
Ir ppm
10
8
6
4
2
0
Au ppm
0.8
0.6
0.4
0.2
0.0
0
5
10
15
Ni wt%
Ni wt%

Figure 6

Table A1. LA-ICP-MS profiles across zoned metal grains in HH 237 and QUE 94627. Errors are 1σ from counting statistics. Data in ppm unless otherwise noted. Italicized entries without uncertainties are detection limits only.

grain #	microns	Ni wt%	Cu	Ga	Ru	Pd	Ir	Au
hh10b	23	6.6 ± 0.6	5.8 ± 0.6	0.33 ± 0.08	4.8 ± 0.5	2.8 ± 0.3	3.2 ± 0.3	0.156 ± 0.024
hh10b	45	7.3 ± 0.7	1.4 ± 0.3	*0.24*	5.2 ± 0.6	3.0 ± 0.3	4.1 ± 0.4	0.059 ± 0.019
hh10b	68	9.8 ± 0.9	2.4 ± 0.4	0.40 ± 0.10	7.4 ± 0.8	3.9 ± 0.4	5.0 ± 0.5	0.043 ± 0.019
hh10b	90	9.6 ± 0.9	2.9 ± 0.4	0.29 ± 0.08	7.0 ± 0.7	3.2 ± 0.3	4.4 ± 0.4	0.036 ± 0.015
hh10b	113	9.0 ± 0.8	1.6 ± 0.3	*0.18*	8.2 ± 0.8	2.9 ± 0.3	3.7 ± 0.4	0.028 ± 0.014
hh10b	135	11.7 ± 1.1	2.4 ± 0.3	*0.20*	8.5 ± 0.9	3.4 ± 0.4	4.2 ± 0.4	0.073 ± 0.018
hh10b	158	12.4 ± 1.1	1.9 ± 0.3	0.23 ± 0.08	9.2 ± 0.9	2.9 ± 0.3	4.4 ± 0.4	0.032 ± 0.015
hh10b	180	11.3 ± 1.0	2.1 ± 0.3	*0.17*	9.6 ± 0.9	3.4 ± 0.4	4.2 ± 0.4	0.031 ± 0.013
hh10b	203	10.5 ± 1.0	1.5 ± 0.2	*0.15*	8.7 ± 0.8	2.9 ± 0.3	4.0 ± 0.4	*0.021*
hh10b	225	12.1 ± 1.1	2.0 ± 0.3	*0.17*	8.8 ± 0.9	3.0 ± 0.3	4.6 ± 0.4	0.028 ± 0.013
hh10b	248	12.9 ± 1.2	2.6 ± 0.3	0.24 ± 0.07	9.3 ± 0.9	3.3 ± 0.3	4.8 ± 0.5	*0.025*
hh10b	270	11.3 ± 1.0	2.9 ± 0.3	*0.17*	8.6 ± 0.8	3.5 ± 0.4	4.8 ± 0.4	0.036 ± 0.013
hh10b	293	9.7 ± 0.9	2.4 ± 0.3	*0.16*	8.0 ± 0.8	3.4 ± 0.4	5.3 ± 0.5	0.039 ± 0.013
hh10b	315	6.8 ± 0.6	9.5 ± 0.9	0.36 ± 0.07	5.2 ± 0.5	3.3 ± 0.3	3.0 ± 0.3	0.059 ± 0.014
hh10d	25	10.5 ± 1.0	6.7 ± 0.7	*0.26*	7.3 ± 0.7	3.7 ± 0.4	3.9 ± 0.4	*0.023*
hh10d	50	10.1 ± 0.9	2.6 ± 0.3	*0.38*	6.8 ± 0.7	3.1 ± 0.3	3.1 ± 0.3	*0.033*
hh10d	75	10.3 ± 0.9	5.3 ± 0.6	0.36 ± 0.09	6.8 ± 0.7	2.9 ± 0.3	3.2 ± 0.3	*0.030*
hh10d	100	8.9 ± 0.8	1.9 ± 0.3	*0.31*	6.4 ± 0.7	2.5 ± 0.3	2.9 ± 0.3	*0.027*
hh10d	125	10.9 ± 1.0	2.0 ± 0.3	*0.37*	7.9 ± 0.8	3.5 ± 0.4	3.6 ± 0.3	*0.033*
hh10d	150	10.2 ± 0.9	2.3 ± 0.3	*0.34*	6.3 ± 0.6	3.0 ± 0.3	3.7 ± 0.4	*0.029*
hh10d	175	11.5 ± 1.1	1.9 ± 0.3	*0.34*	7.4 ± 0.7	3.3 ± 0.4	3.6 ± 0.3	*0.029*
hh10d	200	13.3 ± 1.2	2.4 ± 0.3	*0.41*	9.0 ± 0.9	3.6 ± 0.4	4.6 ± 0.4	*0.036*
hh10d	225	12.6 ± 1.2	1.8 ± 0.3	*0.33*	7.8 ± 0.8	3.2 ± 0.3	3.7 ± 0.4	*0.028*
hh10d	250	11.1 ± 1.0	1.6 ± 0.3	*0.35*	8.6 ± 0.9	3.7 ± 0.4	3.8 ± 0.4	0.033 ± 0.017
hh10d	275	11.0 ± 1.0	1.6 ± 0.2	*0.30*	7.8 ± 0.8	3.5 ± 0.4	3.8 ± 0.4	*0.026*
hh10d	300	10.3 ± 1.0	1.5 ± 0.2	*0.30*	7.2 ± 0.7	3.1 ± 0.3	3.3 ± 0.3	0.047 ± 0.016
hh10d	325	9.3 ± 0.9	1.4 ± 0.2	*0.29*	6.4 ± 0.6	3.0 ± 0.3	3.1 ± 0.3	*0.025*
hh10d	350	10.1 ± 0.9	1.6 ± 0.2	*0.29*	6.9 ± 0.7	3.2 ± 0.3	3.2 ± 0.3	*0.025*
hh10d	375	10.4 ± 1.0	1.6 ± 0.2	*0.31*	7.2 ± 0.7	2.7 ± 0.3	3.5 ± 0.3	*0.027*
hh10d	400	10.4 ± 1.0	1.9 ± 0.3	*0.32*	6.4 ± 0.7	3.3 ± 0.4	3.3 ± 0.3	*0.028*
hh10d	425	8.5 ± 0.8	2.0 ± 0.3	*0.29*	6.0 ± 0.6	2.7 ± 0.3	2.9 ± 0.3	*0.025*
hh11b	25	5.3 ± 0.5	6.3 ± 0.6	0.36 ± 0.07	3.5 ± 0.4	2.9 ± 0.3	2.5 ± 0.2	0.087 ± 0.016
hh11b	50	8.5 ± 0.8	2.1 ± 0.3	*0.28*	5.4 ± 0.6	2.9 ± 0.3	3.8 ± 0.4	0.046 ± 0.014
hh11b	75	9.5 ± 0.9	2.1 ± 0.3	*0.27*	7.7 ± 0.8	3.0 ± 0.3	4.3 ± 0.4	*0.02*
hh11b	100	11.4 ± 1.1	2.0 ± 0.3	*0.25*	9.2 ± 0.9	3.3 ± 0.3	4.4 ± 0.4	0.036 ± 0.013
hh11b	125	12.9 ± 1.2	2.6 ± 0.3	*0.26*	10.0 ± 1.0	4.1 ± 0.4	5.2 ± 0.5	0.026 ± 0.012
hh11b	150	12.0 ± 1.1	2.6 ± 0.3	*0.25*	11.2 ± 1.1	3.3 ± 0.3	5.7 ± 0.5	*0.02*
hh11b	175	13.1 ± 1.2	2.6 ± 0.3	*0.20*	9.4 ± 0.9	3.0 ± 0.3	5.3 ± 0.5	0.024 ± 0.010
hh11b	200	12.8 ± 1.2	2.3 ± 0.3	*0.22*	10.7 ± 1.0	3.6 ± 0.4	5.1 ± 0.5	*0.018*
hh11b	225	11.9 ± 1.1	2.9 ± 0.3	*0.22*	10.5 ± 1.0	3.7 ± 0.4	5.0 ± 0.5	0.021 ± 0.010
hh11b	250	11.0 ± 1.0	2.6 ± 0.3	*0.24*	9.9 ± 1.0	3.2 ± 0.3	5.0 ± 0.5	0.022 ± 0.011
hh11b	275	10.9 ± 1.0	2.8 ± 0.3	*0.23*	8.5 ± 0.8	3.8 ± 0.4	4.9 ± 0.5	0.021 ± 0.011
hh11b	300	8.2 ± 0.8	2.4 ± 0.3	0.24 ± 0.07	6.3 ± 0.6	3.1 ± 0.3	4.1 ± 0.4	0.025 ± 0.011
hh12a	25	5.5 ± 0.5	14.4 ± 1.4	0.50 ± 0.16	4.0 ± 0.4	2.7 ± 0.3	3.3 ± 0.3	0.20 ± 0.03
hh12a	50	7.6 ± 0.7	1.9 ± 0.4	*0.37*	5.1 ± 0.6	2.4 ± 0.3	2.8 ± 0.3	0.06 ± 0.02
hh12a	75	9.7 ± 0.9	2.2 ± 0.4	*0.39*	5.9 ± 0.6	3.2 ± 0.4	2.7 ± 0.3	0.05 ± 0.02
hh12a	100	10.2 ± 0.9	3.1 ± 0.5	*0.37*	6.9 ± 0.7	3.2 ± 0.4	2.9 ± 0.3	*0.04*
hh12a	125	10.6 ± 1.0	2.8 ± 0.4	*0.34*	7.0 ± 0.7	3.4 ± 0.4	3.5 ± 0.3	0.07 ± 0.02
hh12a	150	14.2 ± 1.3	4.5 ± 0.6	*0.35*	9.2 ± 0.9	3.6 ± 0.4	4.5 ± 0.4	0.07 ± 0.02
hh12a	175	13.9 ± 1.3	4.5 ± 0.6	*0.39*	11.0 ± 1.1	3.8 ± 0.4	5.2 ± 0.5	0.05 ± 0.02
hh12a	200	12.6 ± 1.2	3.2 ± 0.4	*0.31*	10.0 ± 1.0	3.9 ± 0.4	5.0 ± 0.5	*0.03*
hh12a	225	12.8 ± 1.2	4.1 ± 0.5	0.41 ± 0.15	10.8 ± 1.1	4.8 ± 0.5	4.8 ± 0.5	0.04 ± 0.02
hh12a	250	12.4 ± 1.1	3.4 ± 0.4	*0.29*	9.3 ± 0.9	3.8 ± 0.4	4.7 ± 0.4	0.06 ± 0.02
hh12a	275	12.6 ± 1.2	3.3 ± 0.4	*0.31*	9.1 ± 0.9	4.8 ± 0.5	5.2 ± 0.5	*0.03*
hh12a	300	13.5 ± 1.2	3.2 ± 0.4	*0.32*	9.9 ± 1.0	4.6 ± 0.5	5.4 ± 0.5	0.07 ± 0.02
hh12a	325	12.4 ± 1.1	3.6 ± 0.5	*0.31*	8.6 ± 0.9	3.9 ± 0.4	4.2 ± 0.4	0.08 ± 0.02
hh12a	350	9.8 ± 0.9	3.7 ± 0.4	0.32 ± 0.13	6.5 ± 0.7	3.3 ± 0.4	3.0 ± 0.3	*0.03*
hh12a	375	9.7 ± 0.9	3.5 ± 0.4	*0.29*	6.9 ± 0.7	3.0 ± 0.3	3.3 ± 0.3	0.03 ± 0.02
hh12a	400	9.1 ± 0.8	6.3 ± 0.7	*0.28*	6.8 ± 0.7	3.1 ± 0.3	3.5 ± 0.3	0.11 ± 0.02
hh14a	24	6.7 ± 0.6	7.1 ± 0.7	0.58 ± 0.13	4.0 ± 0.4	3.1 ± 0.3	3.0 ± 0.3	0.06 ± 0.02
hh14a	48	11.0 ± 1.0	2.2 ± 0.4	0.64 ± 0.17	7.2 ± 0.8	2.9 ± 0.3	5.0 ± 0.5	*0.06*
hh14a	71	10.1 ± 0.9	2.1 ± 0.3	0.46 ± 0.14	8.0 ± 0.8	3.1 ± 0.3	4.4 ± 0.4	*0.05*
hh14a	95	12.0 ± 1.1	2.0 ± 0.3	0.34 ± 0.13	8.7 ± 0.9	3.7 ± 0.4	5.0 ± 0.5	*0.05*
hh14a	119	13.2 ± 1.2	2.9 ± 0.4	*0.37*	10.0 ± 1.0	3.2 ± 0.4	5.9 ± 0.6	*0.06*
hh14a	143	12.1 ± 1.1	2.2 ± 0.3	*0.34*	9.9 ± 1.0	3.6 ± 0.4	5.9 ± 0.6	*0.05*
hh14a	166	12.2 ± 1.1	2.1 ± 0.3	0.38 ± 0.14	10.3 ± 1.0	3.7 ± 0.4	5.7 ± 0.5	*0.05*
hh14a	190	11.5 ± 1.1	1.7 ± 0.3	0.36 ± 0.12	9.3 ± 0.9	3.3 ± 0.4	4.9 ± 0.5	*0.04*
hh14a	214	11.5 ± 1.1	2.3 ± 0.3	0.38 ± 0.14	9.2 ± 0.9	4.1 ± 0.4	5.4 ± 0.5	*0.05*
hh14a	238	9.6 ± 0.9	3.1 ± 0.4	0.37 ± 0.12	7.7 ± 0.8	3.3 ± 0.4	5.0 ± 0.5	*0.05*
hh14a	261	6.8 ± 0.6	3.4 ± 0.4	0.53 ± 0.13	3.9 ± 0.4	3.1 ± 0.3	3.1 ± 0.3	0.07 ± 0.02
hh18b	25	9.4 ± 0.9	3.8 ± 0.4	0.26 ± 0.13	6.9 ± 0.7	2.9 ± 0.3	4.2 ± 0.4	0.03 ± 0.02
hh18b	50	11.7 ± 1.1	2.0 ± 0.4	*0.39*	9.5 ± 1.0	3.0 ± 0.4	4.7 ± 0.4	*0.05*
hh18b	75	12.6 ± 1.2	*1.7*	*0.39*	10.7 ± 1.1	3.3 ± 0.4	6.1 ± 0.6	*0.05*
hh18b	100	13.4 ± 1.2	2.1 ± 0.4	0.41 ± 0.19	11.1 ± 1.1	3.1 ± 0.4	7.1 ± 0.7	*0.05*
hh18b	125	13.5 ± 1.2	2.5 ± 0.4	*0.39*	12.2 ± 1.2	3.7 ± 0.4	7.6 ± 0.7	*0.05*
hh18b	150	11.5 ± 1.1	2.2 ± 0.4	*0.32*	10.8 ± 1.1	3.6 ± 0.4	7.0 ± 0.7	*0.04*
hh18b	175	13.5 ± 1.2	*1.5*	0.41 ± 0.17	10.8 ± 1.1	3.3 ± 0.4	6.1 ± 0.6	*0.04*
hh18b	200	10.7 ± 1.0	1.8 ± 0.3	*0.29*	9.0 ± 0.9	2.9 ± 0.3	4.9 ± 0.5	*0.03*
hh18b	225	10.7 ± 1.0	2.1 ± 0.3	*0.31*	9.1 ± 0.9	4.1 ± 0.4	5.2 ± 0.5	*0.04*
hh18b	250	8.5 ± 0.8	1.8 ± 0.3	*0.32*	6.0 ± 0.6	3.5 ± 0.4	3.9 ± 0.4	*0.04*
hh40b	23	8.7 ± 0.8	*7.9*	*0.92*	7.0 ± 0.8	3.1 ± 0.4	4.0 ± 0.4	*0.23*
hh40b	46	9.9 ± 0.9	*8.4*	*0.98*	10.6 ± 1.1	3.7 ± 0.5	6.2 ± 0.6	*0.24*
hh40b	69	10.8 ± 1.0	*8.1*	*0.94*	11.2 ± 1.2	3.5 ± 0.4	5.5 ± 0.5	*0.23*
hh40b	92	10.0 ± 0.9	*8.0*	*0.93*	10.6 ± 1.1	3.6 ± 0.5	5.0 ± 0.5	*0.23*
hh40b	115	11.3 ± 1.0	*8.5*	*1.00*	10.0 ± 1.1	4.4 ± 0.5	5.9 ± 0.6	*0.24*
hh40b	138	11.3 ± 1.0	*8.4*	*0.97*	10.6 ± 1.1	4.6 ± 0.5	5.7 ± 0.5	*0.24*
hh40b	161	11.7 ± 1.1	*8.4*	*0.98*	11.3 ± 1.2	4.8 ± 0.6	6.5 ± 0.6	*0.24*
hh40b	184	11.6 ± 1.1	*7.6*	*0.89*	11.2 ± 1.2	3.7 ± 0.5	5.4 ± 0.5	*0.22*
que57a	25	5.6 ± 0.5	13.7 ± 1.5	0.55 ± 0.14	3.1 ± 0.4	2.4 ± 0.3	2.2 ± 0.2	*0.12*
que57a	50	6.1 ± 0.6	2.4 ± 0.7	0.36 ± 0.14	3.6 ± 0.4	2.4 ± 0.3	2.5 ± 0.2	*0.13*
que57a	75	8.3 ± 0.8	5.0 ± 1.0	*0.34*	5.2 ± 0.6	2.7 ± 0.3	3.7 ± 0.4	*0.16*
que57a	100	8.7 ± 0.8	3.2 ± 0.9	*0.36*	6.3 ± 0.7	3.2 ± 0.4	3.2 ± 0.3	*0.16*
que57a	125	7.7 ± 0.7	2.1 ± 0.7	*0.27*	5.0 ± 0.6	2.4 ± 0.3	2.7 ± 0.3	*0.12*
que57a	150	8.7 ± 0.8	2.5 ± 0.7	*0.28*	5.4 ± 0.6	2.4 ± 0.3	3.3 ± 0.3	*0.13*
que57a	175	10.8 ± 1.0	3.2 ± 0.8	*0.30*	6.0 ± 0.7	2.9 ± 0.4	3.5 ± 0.3	*0.14*
que57a	200	10.3 ± 1.0	4.9 ± 0.9	*0.29*	6.4 ± 0.7	2.9 ± 0.3	3.8 ± 0.4	*0.13*
que57a	225	11.4 ± 1.1	2.4 ± 0.7	0.38 ± 0.13	7.8 ± 0.8	2.9 ± 0.3	3.6 ± 0.3	*0.13*
que57a	250	11.9 ± 1.1	2.8 ± 0.7	*0.26*	8.0 ± 0.8	3.8 ± 0.4	3.7 ± 0.4	*0.12*
que57a	275	8.6 ± 0.8	2.6 ± 0.6	*0.23*	6.3 ± 0.7	2.9 ± 0.3	3.1 ± 0.3	*0.11*
que57a	300	11.0 ± 1.0	2.5 ± 0.7	*0.27*	8.2 ± 0.9	3.4 ± 0.4	3.7 ± 0.4	*0.13*
que57a	325	12.3 ± 1.1	2.5 ± 0.7	*0.26*	6.7 ± 0.7	3.5 ± 0.4	3.7 ± 0.4	*0.12*
que57a	350	11.1 ± 1.0	2.9 ± 0.7	0.33 ± 0.13	7.2 ± 0.8	3.3 ± 0.4	3.6 ± 0.3	*0.13*
que57a	375	10.3 ± 0.9	4.4 ± 0.8	*0.26*	6.9 ± 0.7	3.5 ± 0.4	4.0 ± 0.4	*0.12*
que57a	400	9.0 ± 0.8	3.3 ± 0.7	0.25 ± 0.11	6.5 ± 0.7	4.0 ± 0.4	3.7 ± 0.4	*0.11*
que57a	425	9.3 ± 0.9	3.1 ± 0.7	*0.26*	5.7 ± 0.6	3.4 ± 0.4	4.0 ± 0.4	*0.12*
que57a	450	7.3 ± 0.7	2.5 ± 0.7	0.32 ± 0.12	4.6 ± 0.5	3.2 ± 0.4	3.3 ± 0.3	*0.12*
que63e	25	6.9 ± 0.6	11.8 ± 1.3	*0.28*	4.3 ± 0.5	3.2 ± 0.4	2.5 ± 0.2	0.13 ± 0.05
que63e	50	9.0 ± 0.8	*1.47*	*0.28*	5.2 ± 0.6	3.6 ± 0.4	4.0 ± 0.4	0.13 ± 0.06
que63e	75	11.9 ± 1.1	2.6 ± 0.8	*0.29*	7.0 ± 0.8	2.6 ± 0.3	5.3 ± 0.5	*0.11*
que63e	100	10.9 ± 1.0	2.0 ± 0.7	*0.27*	9.6 ± 1.0	3.2 ± 0.4	5.6 ± 0.5	*0.10*
que63e	125	11.9 ± 1.1	*1.61*	*0.31*	10.8 ± 1.1	3.3 ± 0.4	6.7 ± 0.6	0.14 ± 0.06
que63e	150	11.4 ± 1.1	*1.40*	*0.27*	11.0 ± 1.1	3.6 ± 0.4	6.2 ± 0.6	*0.10*
que63e	175	10.0 ± 0.9	4.1 ± 0.7	*0.23*	8.0 ± 0.8	2.8 ± 0.3	4.7 ± 0.4	*0.09*
que63e	200	9.6 ± 0.9	1.8 ± 0.7	*0.25*	7.0 ± 0.7	3.1 ± 0.4	4.7 ± 0.4	0.13 ± 0.05
que63e	225	7.4 ± 0.7	2.4 ± 0.6	*0.21*	5.3 ± 0.6	2.8 ± 0.3	3.5 ± 0.3	*0.08*
que63e	250	5.9 ± 0.5	3.6 ± 0.6	*0.20*	3.8 ± 0.4	3.0 ± 0.3	2.5 ± 0.2	*0.08*